Radboud Repository

Radboud University Nijmegen

PDF hosted at the Radboud Repository of the Radboud University Nijmegen

The following full text is a publisher's version.

For additional information about this publication click this link.
http://hdl.handle.net/2066/129376

A search for neutral Higgs particles in Z^0 decays

DELPHI Collaboration

P. Abreu [r], W. Adam [ar], F. Adami [ai], T. Adye [ag], T. Akesson [u], G.D. Alekseev [m], P. Allen [aq], S. Almehed [u], S.J. Alvsvaag [d], U. Amaldi [g], E. Anassontzis [c], P. Antilogus [v], W-D. Apel [n], R.J. Apsimon [ag], B. Åsman [am], P. Astier [t], J-E. Augustin [p], A. Augustinus [ab], P. Baillon [g], P. Bambade [p], F. Barao [r], R. Barate [k], G. Barbiellini [ao], D.Y. Bardin [m], A. Baroncelli [aj], O. Barring [u], W. Bartl [ar], M.J. Bates [ae], M. Battaglia [z], M. Baubillier [t], K-H. Becks [at], C.J. Beeston [ae], M. Begalli [j], P. Beilliere [f], Yu. Belokopytov [al], P. Beltran [i], D. Benedic [h], J.M. Benlloch [aq], M. Berggren [am], D. Bertrand [b], F. Bianchi [an], M.S. Bilenky [m], P. Billoir [t], J. Bjarne [u], D. Bloch [h], S. Blyth [ae], V. Bocci [ah], P.N. Bogolubov [m], T. Bolognese [ai], M. Bonapart [ab], M. Bonesini [z], W. Bonivento [z], P.S.L. Booth [s], B. Bostjancic [g], O. Botner [ap], B. Bouquet [p], M. Bozzo [j], S. Braibant [b], P. Branchini [aj], K.D. Brand [af], R.A. Brenner [l], C. Bricman [b], R.C.A. Brown [g], N. Brummer [ab], J-M. Brunet [f], L. Bugge [ad], T. Buran [ad], H. Burmeister [g], J.A.M.A. Buytaert [g], M. Caccia [g], M. Calvi [z], A.J. Camacho Rozas [ak], A. Campion [s], T. Camporesi [g], V. Canale [ah], F. Cao [b], F. Carena [g], L. Carroll [s], C. Caso [j], E. Castelli [ao], M.V. Castillo Gimenez [aq], A. Cattai [g], F.R. Cavallo [e], L. Cerrito [ah], A. Chan [a], P. Charpentier [g], P. Checchia [af], G.A. Chelkov [m], L. Chevalier [ai], P. Chliapnikov [al], V. Chorowicz [t], R. Cirio [an], M.P. Clara [an], P. Collins [ae], J.L. Contreras [w], R. Contri [j], G. Cosme [p], F. Couchot [p], H.B. Crawley [a], D. Crennell [ag], G. Crosetti [j], M. Crozon [f], J. Cuevas Maestro [ak], S. Czellar [l], S. Dagoret [p], E. Dahl-Jensen [aa], B. Dalmagne [p], M. Dam [d], G. Damgaard [aa], G. Darbo [j], E. Daubie [b], P.D. Dauncey [ae], M. Davenport [g], P. David [t], A. De Angelis [ao], M. De Beer [ai], H. De Boeck [b], W. De Boer [n], C. De Clercq [b], M.D.M. De Fez Laso [aq], N. De Groot [ab], C. De La Vaissiere [t], B. De Lotto [ao], A. De Min [z], C. Defoix [f], D. Delikaris [g], S. Delorme [g], P. Delpierre [f], N. Demaria [an], J. Derkaoui [an,x], L. Di Ciaccio [ah], H. Dijkstra [g], F. Djama [h], J. Dolbeau [f], O. Doll [at], M. Donszelmann [ab], K. Doroba [as], M. Dracos [g], J. Drees [at], M. Dris [ac], Y. Dufour [f], W. Dulinski [h], L-O. Eek [ap], P.A.-M. Eerola [g], T. Ekelof [ap], G. Ekspong [am], A. Elliot Peisert [af], J-P. Engel [h], D. Fassouliotis [ac], M. Feindt [g], A. Fenyuk [al], M. Fernandez Alonso [ak], A. Ferrer [aq], T.A. Filippas [ac], A. Firestone [a], H. Foeth [g], E. Fokitis [ac], P. Folegati [ao], F. Fontanelli [j], K.A.J. Forbes [s], H. Forsbach [at], B. Franek [ag], P. Frenkiel [f], D.C. Fries [n], A.G. Frodesen [d], R. Fruhwirth [ar], F. Fulda-Quenzer [p],

K. Furnival [s], H. Furstenau [n], J. Fuster [g], G. Galeazzi [af], D. Gamba [an],
C. Garcia [aq], J. Garcia [ak], C. Gaspar [g], U. Gasparini [af], P. Gavillet [g], E.N. Gazis [ac],
J-P. Gerber [h], P. Giacomelli [g], K-W. Glitza [at], R. Gokieli [g], V.M. Golovatyuk [m],
J.J. Gomez Y Cadenas [g], A. Goobar [am], G. Gopal [ag], M. Gorski [as], V. Gracco [j],
A. Grant [g], F. Grard [b], E. Graziani [aj], M-H. Gros [p], G. Grosdidier [p], E. Gross [g],
B. Grossetete [t], P. Grosse-Wiesmann [g], S. Gumenyuk [al], J. Guy [ag], F. Hahn [g],
M. Hahn [n], S. Haider [ab], Z. Hajduk [ab], A. Hakansson [u], A. Hallgren [ap],
K. Hamacher [at], G. Hamel De Monchenault [ai], F.J. Harris [ae], B.W. Heck [g],
T. Henkes [g], I. Herbst [at], J.J. Hernandez [aq], P. Herquet [b], H. Herr [g], I. Hietanen [l],
C.O. Higgins [s], E. Higon [aq], H.J. Hilke [g], S.D. Hodgson [ae], T. Hofmokl [as],
R. Holmes [a], S-O. Holmgren [am], D. Holthuizen [ab], P.F. Honore [f], J.E. Hooper [aa],
M. Houlden [s], J. Hrubec [ar], P.O. Hulth [am], K. Hultqvist [am], D. Husson [h],
P. Ioannou [c], D. Isenhower [g], P-S. Iversen [d], J.N. Jackson [s], P. Jalocha [o],
G. Jarlskog [u], P. Jarry [ai], B. Jean-Marie [p], E.K. Johansson [am], D. Johnson [s],
M. Jonker [g], L. Jonsson [u], P. Juillot [h], G. Kalkanis [c], G. Kalmus [ag], F. Kapusta [t],
S. Katsanevas [c], E.C. Katsoufis [ac], R. Keranen [l], J. Kesteman [b], B.A. Khomenko [m],
N.N. Khovanski [m], B. King [s], N.J. Kjaer [g], H. Klein [g], W. Klempt [g], A. Klovning [d],
P. Kluit [ab], A. Koch-Mehrin [at], J.H. Koehne [n], B. Koene [ab], P. Kokkinias [i],
M. Kopf [n], M. Koratzinos [an], K. Korcyl [o], A.V. Korytov [m], M. Kostrikov [al],
C. Kourkoumelis [c], T. Kreuzberger [ar], J. Krolikowski [as], I. Kronkvist [u], J. Krstic [ae],
U. Kruener-Marquis [at], W. Krupinski [o], W. Kucewicz [z], K. Kurvinen [l],
C. Lacasta [aq], C. Lambropoulos [i], J.W. Lamsa [a], L. Lanceri [ao], V. Lapin [al],
J-P. Laugier [ai], R. Lauhakangas [l], G. Leder [ar], F. Ledroit [k], R. Leitner [g],
Y. Lemoigne [ai], J. Lemonne [b], G. Lenzen [at], V. Lepeltier [p], A. Letessier-Selvon [t],
D. Liko [ar], E. Lieb [at], E. Lillethun [d], J. Lindgren [l], A. Lipniacka [as], I. Lippi [af],
R. Llosa [w], B. Loerstad [u], M. Lokajicek [m], J.G. Loken [ae], M.A. Lopez Aguera [ak],
A. Lopez-Fernandez [p], M. Los [ab], D. Loukas [i], A. Lounis [h], J.J. Lozano [aq],
R. Lucock [ag], P. Lutz [f], L. Lyons [ae], G. Maehlum [g], N. Magnussen [at], J. Maillard [f],
A. Maltezos [i], F. Mandl [ar], J. Marco [ak], M. Margoni [af], J-C. Marin [g], A. Markou [i],
S. Marti [aq], L. Mathis [f], F. Matorras [ak], C. Matteuzzi [z], G. Matthiae [ah],
M. Matveev [al], M. Mazzucato [af], M. Mc Cubbin [s], R. Mc Kay [a], R. Mc Nulty [s],
E. Menichetti [an], G. Meola [j], C. Meroni [z], W.T. Meyer [a], M. Michelotto [af],
W.A. Mitaroff [ar], G.V. Mitselmakher [m], U. Mjoernmark [u], T. Moa [am],
R. Moeller [aa], K. Moenig [g], M.R. Monge [j], P. Morettini [j], H. Mueller [n],
W.J. Murray [ag], G. Myatt [ae], F. Naraghi [t], U. Nau-Korzen [at], F.L. Navarria [e],
P. Negri [z], B.S. Nielsen [aa], B. Nijjhar [s], V. Nikolaenko [al], V. Obraztsov [al],
A.G. Olshevski [m], R. Orava [l], A. Ostankov [al], A. Ouraou [ai], M. Paganoni [z],
R. Pain [t], H. Palka [ab], T. Papadopoulou [ac], L. Pape [g], A. Passeri [aj], M. Pegoraro [af],
V. Perevozchikov [al], M. Pernicka [ar], A. Perrotta [e], F. Pierre [ai], M. Pimenta [r],
O. Pingot [b], M.E. Pol [g], G. Polok [o], P. Poropat [ao], P. Privitera [n], A. Pullia [z],
J. Pyyhtia [l], D. Radojicic [ae], S. Ragazzi [z], P.N. Ratoff [q], A.L. Read [ad],
N.G. Redaelli [z], M. Regler [ar], D. Reid [s], P.B. Renton [ae], L.K. Resvanis [c],

F. Richard [p], M. Richardson [s], J. Ridky [m], G. Rinaudo [an], I. Roditi [g],
A. Romero [an], I. Roncagliolo [j], P. Ronchese [af], C. Ronnqvist [l], E.I. Rosenberg [a],
U. Rossi [e], E. Rosso [g], P. Roudeau [p], T. Rovelli [e], W. Ruckstuhl [ab],
V. Ruhlmann [ai], A. Ruiz [ak], K. Rybicki [o], H. Saarikko [l], Y. Sacquin [ai], G. Sajot [k],
J. Salt [aq], E. Sanchez [aq], J. Sanchez [w], M. Sannino [j], M. Schaeffer [h], S. Schael [n],
H. Schneider [n], M.A.E. Schyns [g], F. Scuri [ao], A.M. Segar [ae], R. Sekulin [ag],
M. Sessa [ao], G. Sette [j], R. Seufert [n], R.C. Shellard [g], P. Siegrist [ai], S. Simonetti [j],
F. Simonetto [af], A.N. Sissakian [m], T.B. Skaali [ad], G. Skjevling [ad], G. Smadja [ai,v],
G.R. Smith [ag], N. Smirnov [al], R. Sosnowski [as], T.S. Spassoff [k], E. Spiriti [aj],
S. Squarcia [j], H. Staeck [at], C. Stanescu [aj], G. Stavropoulos [i], F. Stichelbaut [b],
A. Stocchi [p], J. Strauss [ar], R. Strub [h], M. Szczekowski [as], M. Szeptycka [as],
P. Szymanski [as], T. Tabarelli [z], S. Tavernier [b], G. Theodosiou [i], A. Tilquin [y],
J. Timmermans [ab], V.G. Timofeev [m], L.G. Tkatchev [m], T. Todorov [m],
D.Z. Toet [ab], L. Tortora [aj], M.T. Trainor [ae], D. Treille [g], U. Trevisan [j],
W. Trischuk [g], G. Tristram [f], C. Troncon [z], A. Tsirou [g], E.N. Tsyganov [m],
M. Turala [o], R. Turchetta [h], M-L. Turluer [ai], T. Tuuva [l], I.A. Tyapkin [m],
M. Tyndel [ag], S. Tzamarias [g], B. Ueberschaer [at], S. Ueberschaer [at], O. Ullaland [g],
V.A. Uvarov [al], G. Valenti [e], E. Vallazza [an], J.A. Valls Ferrer [aq],
G.W. Van Apeldoorn [ab], P. Van Dam [ab], W.K. Van Doninck [b], C. Vander Velde [b],
J. Varela [r], P. Vaz [g], G. Vegni [z], L. Ventura [af], W. Venus [ag], F. Verbeure [b],
L.S. Vertogradov [m], L. Vibert [t], D. Vilanova [ai], L. Vitale [ao], E.V. Vlasov [al],
S. Vlassopoulos [ac], A.S. Vodopyanov [m], M. Vollmer [at], S. Volponi [e],
G. Voulgaris [c], M. Voutilainen [l], V. Vrba [aj], H. Wahlen [at], C. Walck [am],
F. Waldner [ao], M. Wayne [a], P. Weilhammer [g], J. Werner [at], A.M. Wetherell [g],
J.H. Wickens [b], J. Wikne [ad], G.R. Wilkinson [ae], W.S.C. Williams [ae], M. Winter [h],
D. Wormald [ad], G. Wormser [p], K. Woschnagg [ap], N. Yamdagni [am], P. Yepes [g],
A. Zaitsev [al], A. Zalewska [o], P. Zalewski [as], D. Zavrtanik [g], E. Zevgolatakos [i],
G. Zhang [at], N.I. Zimin [m], M. Zito [ai], R. Zitoun [t], R. Zukanovich Funchal [f],
G. Zumerle [af] and J. Zuniga [aq]

[a] *Ames Laboratory and Department of Physics, Iowa State University, Ames, IA 50011, USA.*
[b] *Physics Department, Univ. Instelling Antwerpen, Universiteitsplein 1, B-2610 Wilrijk, Belgium*
and IIHE, ULB-VUB, Pleinlaan 2, B-1050 Brussels, Belgium
and Service de Phys. des Part. Elém., Faculté des Sciences, Université de l'Etat Mons, Av. Maistriau 19,
B-7000 Mons, Belgium.
[c] *Physics Laboratory, University of Athens, Solonos Str. 104, GR-10680 Athens, Greece.*
[d] *Department of Physics, University of Bergen, Allégaten 55, N-5007 Bergen, Norway.*
[e] *Dipartimento di Fisica, Università di Bologna and INFN, Via Irnerio 46, I-40126 Bologna, Italy.*
[f] *Collège de France, Lab. de Physique Corpusculaire, 11 pl. M. Berthelot, F-75231 Paris Cedex 05, France.*
[g] *CERN, CH-1211 Geneva 23, Switzerland.*
[h] *Division des Hautes Energies, CRN - Groupe DELPHI and LEPSI, B.P.20 CRO,*
F-67037 Strasbourg Cedex, France.
[i] *Institute of Nuclear Physics, N.R.C. Demokritos, P.O. Box 60628, GR-15310 Athens, Greece.*
[j] *Dipartimento di Fisica, Università di Genova and INFN, Via Dodecaneso 33, I-16146 Genoa, Italy.*
[k] *Institut des Sciences Nucléaires, Université de Grenoble 1, F-38026 Grenoble, France.*
[l] *Research Institute for High Energy Physics, University of Helsinki, Siltavuorenpenger 20 C,*
SF-00170 Helsinki 17, Finland.

^{m} *Joint Institute for Nuclear Research, Dubna, Head Post Office, P.O. Box 79, 101 000 Moscow, USSR.*
^{n} *Institut für Experimentelle Kernphysik, Universität Karlsruhe, Postfach 6980, D-7500 Karlsruhe 1, Germany.*
^{o} *High Energy Physics Laboratory, Institute of Nuclear Physics, Ul. Kawiory 26 a, PL-30055 Krakow 30, Poland.*
^{p} *Université de Paris-Sud, Lab. de l'Accélérateur Linéaire, Bat 200, F-91405 Orsay, France.*
^{q} *School of Physics and Materials, University of Lancaster - Lancaster LA1 4YB, UK.*
^{r} *LIP, Av. Elias Garcia 14 - 1e, P-1000 Lisbon Codex, Portugal.*
^{s} *Department of Physics, University of Liverpool, P.O. Box 147, GB - Liverpool L69 3BX, UK.*
^{t} *LPNHE, Universités Paris VI et VII, Tour 33 (RdC), 4 place Jussieu, F-75230 Paris Cedex 05, France.*
^{u} *Department of Physics, University of Lund, Sölvegatan 14, S-22363 Lund, Sweden.*
^{v} *Université Claude Bernard de Lyon, 43 Bd du 11 Novembre 1918, F-69622 Villeurbanne Cedex, France.*
^{w} *Universidad Complutense, Avda. Complutense s / n, E-28040 Madrid, Spain.*
^{x} *Permanent address: Département de Physique, Faculté des Sciences d'Oujda, Maroc.*
^{y} *Univ. d'Aix - Marseille II - Case 907 - 70, route Léon Lachamp, F-13288 Marseille Cedex 09, France.*
^{z} *Dipartimento di Fisica, Università di Milano and INFN, Via Celoria 16, I-20133 Milan, Italy.*
^{aa} *Niels Bohr Institute, Blegdamsvej 17, DK-2100 Copenhagen ø, Denmark.*
^{ab} *NIKHEF-H, Postbus 41882, NL-1009 DB Amsterdam, The Netherlands.*
^{ac} *National Technical University, Physics Department, Zografou Campus, GR-15773 Athens, Greece.*
^{ad} *Physics Department, University of Oslo, Blindern, N-1000 Oslo 3, Norway.*
^{ac} *Nuclear Physics Laboratory, University of Oxford, Keble Road, GB - Oxford OX1 3RH, UK.*
^{af} *Dipartimento di Fisica, Università di Padova and INFN, Via Marzolo 8, I-35131 Padua, Italy.*
^{ag} *Rutherford Appleton Laboratory, Chilton, GB - Didcot OX11 OQX, UK.*
^{ah} *Dipartimento di Fisica, Università di Roma II and INFN, Tor Vergata, I-00173 Rome, Italy.*
^{ai} *CEN-Saclay, DPhPE, F-91191 Gif-sur-Yvette Cedex, France.*
^{aj} *Istituto Superiore di Sanità, Ist. Naz. di Fisica Nucl. (INFN), Viale Regina Elena 299, I-00161 Rome, Italy.*
^{ak} *Facultad de Ciencias, Universidad de Santander, av. de los Castros, E-39005 Santander, Spain.*
^{al} *Inst. for High Energy Physics, Serpukow, P.O. Box 35, Protvino (Moscow Region), USSR.*
^{am} *Institute of Physics, University of Stockholm, Vanadisvägen 9, S-113 46 Stockholm, Sweden.*
^{an} *Dipartimento di Fisica Sperimentale, Università di Torino and INFN, Via P. Giuria 1, I-10125 Turin, Italy.*
^{ao} *Dipartimento di Fisica, Università di Trieste and INFN, Via A. Valerio 2, I-34127 Trieste, Italy and Istituto di Fisica, Università di Udine, I-33100 Udine, Italy.*
^{ap} *Department of Radiation Sciences, University of Uppsala, P.O. Box 535, S-751 21 Uppsala, Sweden.*
^{aq} *Inst. de Fisica Corpuscular IFIC, Centro Mixto Univ. de Valencia-CSIC, and Departamento de Fisica Atomica Molecular y Nuclear, Univ. de Valencia, Avda. Dr. Moliner 50, E-46100 Burjassot (Valencia), Spain.*
^{ar} *Institut für Hochenergiephysik, Österreich Akad. d. Wissensch., Nikolsdorfergasse 18, A-1050 Vienna, Austria.*
^{as} *Inst. Nuclear Studies and, University of Warsaw, Ul. Hoza 69, PL-00681 Warsaw, Poland.*
^{at} *Fachbereich Physik, University of Wuppertal, Postfach 100 127, D-5600 Wuppertal 1, Germany.*

The search in DELPHI data for neutral Higgs bosons is described. No candidate for the Standard Model Higgs is seen in Z^0 decays to $H^0 \nu \bar{\nu}$, $H^0 \mu^+ \mu^-$ or $H^0 \tau^+ \tau^-$ after selections that proved efficient for finding simulated H^0. One remaining candidate for $Z^0 \to H^0 e^+ e^-$ is consistent with background. Together with our earlier studies, these results restrict the H^0 mass to be above 38 GeV/c^2 at the 95% confidence level. No signal is found for decays of Minimal Supersymmetric Standard Model neutral Higgs bosons to $\tau^+ \tau^-$. Limits are obtained for their decays to produce four jets.

1. Introduction

The Standard Model [1] predicts the existence of a neutral scalar Higgs particle, H^0, and its couplings to quarks and leptons. However the H^0 mass, m_{H^0}, is not predicted. The Higgs [2] mechanism remains an unverified but essential ingredient of the Standard Model (SM) and its supersymmetric extensions.

Several searches [3] for the Higgs boson were reported before LEP started providing Z^0. However the interpretation of the searches were subject to significant uncertainties for masses outside the region 1.2 to 52 MeV/c^2 [4].

The experiments at LEP take advantage of the expected production of the Standard Model H^0 by

$$e^+e^- \to Z^0 \to H^0 + Z^{0*}, \qquad Z^{0*} \to q\bar{q} \text{ or } \ell\bar{\ell} \qquad (1)$$

where the virtual Z^{0*} giving an $\ell\bar{\ell}$ lepton pair in the final state is generally used as a signature for Z^0 decays that produce H^0. The H^0 mass was restricted to be small or above about 14 to 20 GeV/c^2 by searches in Z^0 decays from the limited statistics of the 1989 data [5–7]. Furthermore, including the 1990 data, the Higgs boson was excluded down to zero mass [8–11]. It remains to look for H^0 up to the highest masses which become accessible as larger data samples are available.

Here we present results, obtained with the DELPHI detector, for reaction (1) with $Z^{0*} \to \nu\bar{\nu}$, e^+e^-, $\mu^+\mu^-$ and $\tau^+\tau^-$, for m_{H^0} between 12 and 45 GeV/c^2. For these masses the dominant H^0 decay would be to $b\bar{b}$ pairs, the heaviest available particles, seen as hadron jets with several charged particles. Also $H^0 \to \tau^+\tau^-$ would be present with a branching ratio of some 6%.

Events with an H^0 and $Z^{0*} \to \nu\bar{\nu}$ pair would be distinguished by only having the H^0 decay products detected, with the remaining energy and momentum unseen. Final states with charged leptons have a smaller branching ratio. They are distinguished by a lepton pair well isolated from the hadronic remnants from the H^0.

In principle one may also search for H^0 production when both H^0 and Z^{0*} decay to $q\bar{q}$ with four jets in the final state. However we found that any H^0 peak would not be well resolved from background mass combinations with these data.

In the Minimal Supersymmetric extension to the Standard Model (MSSM) there are two complex Higgs doublets which give rise to five physical Higgs bosons (H^+, H^-, h^0, $\mathscr{H}^0$, A^0) [12]. There are two CP-even scalars h^0 and $\mathscr{H}^0$, which mix with an angle α, and one CP-odd pseudoscalar A^0. The model is fully specified by two parameters. These can be chosen to be m_h (the mass of the lightest scalar) and $\tan\beta = v_2/v_1$; v_1 and v_2 are the vacuum expectation values of the Higgs fields which couple only to down-type quarks and charged leptons or to up-type quarks and neutrinos, respectively. In the Born approximation, the masses are constrained

such that m_{H^+} is larger than m_W and m_h is smaller than $m_Z|\cos 2\beta|$, although this is no longer true at higher order [13]. Note that in the limit when m_A becomes large, $\tan \beta$ approaches 1, and h^0 becomes equivalent to the Standard Model Higgs particle.

Production of MSSM neutral Higgs particles is predicted to occur predominantly by two complementary production mechanisms:

$$e^+e^- \to h^0 Z^{0*} \quad \text{or} \quad e^+e^- \to Z^0 \to h^0 A^0,$$

with cross sections proportional to $\sin^2(\alpha - \beta)\sigma_{H^0}$ and $\cos^2(\alpha - \beta)\sigma_{\nu\bar{\nu}}$ where the SM cross sections σ_{H^0} and $\sigma_{\nu\bar{\nu}}$ are for $e^+e^- \to Z^0 \to H^0 Z^{0*}$ and $e^+e^- \to Z^0 \to \nu\bar{\nu}$. In the model

$$\cos^2(\alpha - \beta) = \frac{m_h^2(m_Z^2 - m_h^2)}{m_A^2(m_Z^2 + m_A^2 - 2m_h^2)}$$

The h^0 and A^0 decay modes of interest in the search are into heavy $f\bar{f}$ pairs which are kinematically allowed. The branching ratios depend strongly on α and β:

$$BR(h^0 \to \tau\bar{\tau}:c\bar{c}:b\bar{b}) = 1:2.1(\cot \alpha \cot \beta)^2:19\beta_b^3,$$

$$BR(A^0 \to \tau\bar{\tau}:c\bar{c}:b\bar{b}) = 1:2.1(\cot \beta)^4:19\beta_b^3,$$

where β_b is the b-quark velocity in the Higgs rest frame. Since the mixing angle α is approximately equal to $-\beta$ in the mass range considered here, the decay fractions for h^0 and A^0 are roughly similar. For $\tan \beta$ much larger than 1, $\tau^+\tau^-$ and $b\bar{b}$ dominate. The $\tau^+\tau^-$ mode is still appreciable (4% to 5%) even far above the $b\bar{b}$ threshold. For $\tan \beta$ much less than 1 the $c\bar{c}$ mode dominates – with some admixture of $b\bar{b}$ for $\tan \beta$ near 1, corresponding to mass differences between h^0 and the A^0 of 5 GeV/c^2 or more.

Thus in the MSSM model, the search for the SM H^0 already restricts the possible values of m_h, if $\tan \beta$ were about 1. There can be extra Z^0 decays with τ pairs if $\tan \beta$ were above 1, or with four jets with di-jet masses peaking at m_h and m_A if $\tan \beta$ were above or below 1. Searches for such decays in the 1989 data from DELPHI are described in ref. [14].

2. Data

The present analysis is based on data collected by DELPHI during the 1990 scans at LEP around the Z^0 peak. Some 119 000 hadronic Z^0 decays were

detected, depending on specific selections on the data taking conditions. A summary of specific properties of the DELPHI detector [15] relevant to this analysis follows.

Charged particle tracks are measured in the 1.2 Tesla magnetic field by three cylindrical tracking chambers: the Inner Detector (ID) at radii 12 to 28 cm, the Time Projection Chamber (TPC), the main tracking device, covers radii 30 to 122 cm and the Outer Detector (OD) 197 to 208 cm. Beyond the solenoid coil are Time of Flight (TOF) counters for triggering. The Forward Chambers A and B, cover polar angles 10° to 30° and 150° to 170°.

Electromagnetic energy is measured by the High density Projection Chamber (HPC) in the barrel and by the Forward ElectroMagnetic Calorimeter (FEMC). The HPC has layers of lead and gas covering polar angles from 40° to 140°. A scintillation layer is installed after the first 5 radiation lengths for fast triggering. The FEMC has lead glass blocks covering polar angles 10° to 36° and 144° to 170°.

Hadron shower energies are measured by combining measurements from the Hadron Calorimeter (the instrumented iron return yoke for the magnet) and the electromagnetic calorimeters.

Muons are identified by their penetration through the yoke to the MUon Barrel and Forward chambers (MUB and MUF) which have layers inside and outside the iron yoke. The calorimeters also distinguish hadron or electromagnetic showers from muons.

The Small Angle Tagger (SAT) measures the luminosity and is also used to veto significant energy seen at a small angle to either beam.

The trigger is based on ID and OD coincidences, on the HPC and TOF scintillation counters, and on the forward detectors. The trigger efficiency for events with H^0 in the mass range studied is indistinguishable from that for hadronic events which is greater than 99.7% [16].

Monte Carlo data samples included $Z^0 \rightarrow H^0 + Z^0*$ for several H^0 masses with of the order of 1000 events simulated at each mass (and h^0A^0 production for MSSM), and possible background contributions from some 110000 simulated $Z^0 \rightarrow q\bar{q}$, 11000 $\tau^+\tau^-$ and 22000 $\mu^+\mu^-$ decays. These were used to define the selection criteria and determine their efficiencies. H^0 production processes were generated [17] and then fragmentation was simulated using the LUND parton shower model [18] and the results passed through the DELPHI detailed simulation program. This produces the expected signals in the various subelements of the detectors. The simulated raw data for these samples were passed through the same reconstruction and analysis programs as real data.

The Standard Model parameters obtained from DELPHI [16] data were used to predict the cross sections for H^0 production [19,20], 5.5 pb at the Z^0 for $m_{H^0} = 40$ GeV/c^2. The calculation included initial-state radiative corrections computed with exponentiation and a triangle vertex correction with a top quark of mass 200 GeV/c^2.

3. Search for $Z^0 \to H^0 + \nu + \bar{\nu}$

Due to the large missing momentum carried by the two neutrinos, the $Z^0 \to H^0 Z^{0*}$, $Z^{0*} \to \nu\bar{\nu}$ decays very often appear unbalanced. This is the main feature used to distinguish these from the majority of $Z^0 \to q\bar{q}$ decays.

Detection of particles and measurement of energy are particularly important, as missing momentum is one of the selection criteria. We therefore require that the TPC and all calorimeters were working.

The reconstructed mass, m_r, of most $Z^0 \to q\bar{q}$ is much larger than a Higgs with mass 45 GeV/c^2. However the decay $Z^0 \to \tau^+\tau^-$ may produce potential background candidates due to the missing momentum carried by the neutrinos from the τ decays. These events are efficiently suppressed by selecting charged multiplicities, n_{ch}, above 6 and removing such typically back-to-back events. In contrast, the charged multiplicity of most H^0 decays is quite large when m_{H^0} is large enough for decay to $b\bar{b}$. Background events from beam–gas and beam–wall interactions are eliminated by selecting candidates with the particles produced at a large angle to the beam.

To reduce the background further a set of topological variables are used. These variables exploit the fact that the Higgs boson events, as opposed to the background, have a pronounced spatial asymmetry in the laboratory system due to the (invisible) neutrinos. We use the acoplanarity and λ, ρ and E_{50} as defined below.

To calculate the acoplanarity the event is split into two hemispheres divided by a plane perpendicular to the thrust axis. The sum of particle momenta in each hemisphere is projected onto the plane perpendicular to the beam axis. Acoplanarity is defined as the complement of the angle between the two sums. If all the energy is in one hemisphere, we take the acoplanarity as 90°.

λ is the angle between the direction of missing momentum and the closest reconstructed jet. Jets are defined with the algorithm LUCLUS [18].

ρ is the complement of the largest angle between any two jets, for events with three or more jets with an energy above 2 GeV.

E_{50} is the total energy of reconstructed particles in a cone with 50° half angle about the missing momentum.

The search is divided into two complementary sets of selections; *analysis I* has a reasonably good efficiency for Higgs boson masses from 10 to 40 GeV/c^2, while *analysis II* is optimised for heavier Higgs masses, up to 50 GeV/c^2.

Both analyses initially use charged particles (with momentum above 100 MeV/c) as well as showers with energy above 100 MeV (which are not linked to a charged particle). Candidates must have n_{ch} above 6 and an energy sum of these charged particles (assumed to be pions) above 8 GeV, missing transverse momentum (with respect to the beam) above 5 GeV/c and missing momentum, P_{mis}, at more than 18° to the beam axis. Hadronic Z^0 decays with high-momentum charged secondaries can be reconstructed with a large momentum imbalance due to the occa-

sional deterioration in momentum resolution for shorter, straighter tracks. To remove this background the particle with highest momentum (above 7 GeV/c) must have fractional momentum error below 1. For Higgs masses considered here the signal is no longer that of a strongly boosted hadronic system. So we reject contamination from beam related background and $Z^0 \to q\bar{q}\gamma$ (with a high-energy γ) by requiring $|P_{mis}|$ to be below 35 GeV/c and, for m_r above 10 GeV/c^2, $|P_{mis}|$ to be less than $0.8 \times E_{vis}$ (where E_{vis} is the measured energy of all the detected charged and neutral particles.) In addition events with more than 10% of their recorded energy going in the forward and backward directions (within 15° of the beam axis) are rejected since these events may have missed an important amount of energy along the beam pipe.

After the initial selections, events are removed in *analysis I* when significant energy is seen in the regions where the detectors have incomplete coverage. The sum of the energy in all SAT detectors is required to be below 4 GeV and the thrust axis and P_{mis} to be at more than 25° to the beam. If m_r is below 10 GeV/c^2 then all particles must be in one hemisphere.

Comparison of the differential distributions for the simulated $Z^0 \to q\bar{q}$ and $\tau\bar{\tau}$ backgrounds and the possible $Z^0 \to H^0\nu\bar{\nu}$ signal led to selections that optimise background rejection and H^0 acceptance. Fig. 1 and table 1 show the effects of the sequential selections on the data, on simulated Z^0 decays initially normalised to the data, and on H^0 with a mass of 40 GeV/c^2. After the preselections described above, the remaining events must have:

(a) ρ above 30° for events with more than two jets, fig. 1a;
(b) λ above 42°, fig. 1b;
(c) acoplanarity above 15° (or 30° if m_r below 25 GeV/c^2), fig. 1c;
(d) m_r below 40 GeV/c^2, fig. 1d.

TABLE 1

The numbers of events remaining after $Z^0 \to H^0\nu\bar{\nu}$ sequential selections on the data, and on a Monte Carlo background sample normalised to the number of hadronic Z^0 decays in the initial data sample

Selection	Real data	Simulated $Z^0 \to q\bar{q}$	$m_{H^0} = 40\,\mathrm{GeV}/c^2$
Analysis-I preselections	56132	51080	2.9
$\rho > 30°$	13380	15205	2.6
$\lambda > 42°$	685	671	2.4
acoplanarity $> 15°$	160	161	2.2
$m_r < 40\,\mathrm{GeV}/c^2$	0	1	2.1
Analysis-II preselections	60419	54127	3.1
acoplanarity $> 2.5°$	32791	27401	3.1
$\rho > 36°$	5138	5538	2.7
$E_{50} < 1\,\mathrm{GeV}$	63	64	2.0
$m_r < 45\,\mathrm{GeV}/c^2$	0	2	1.9

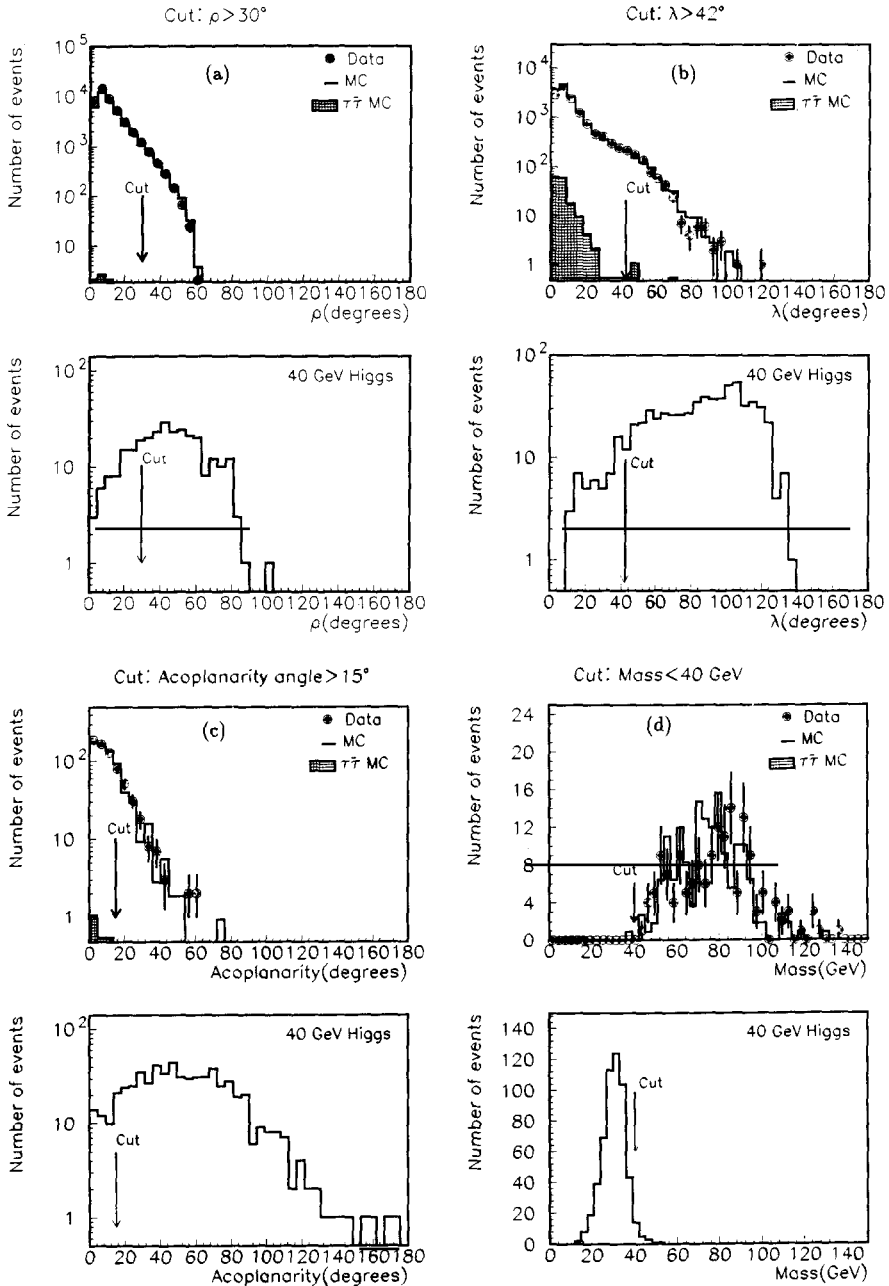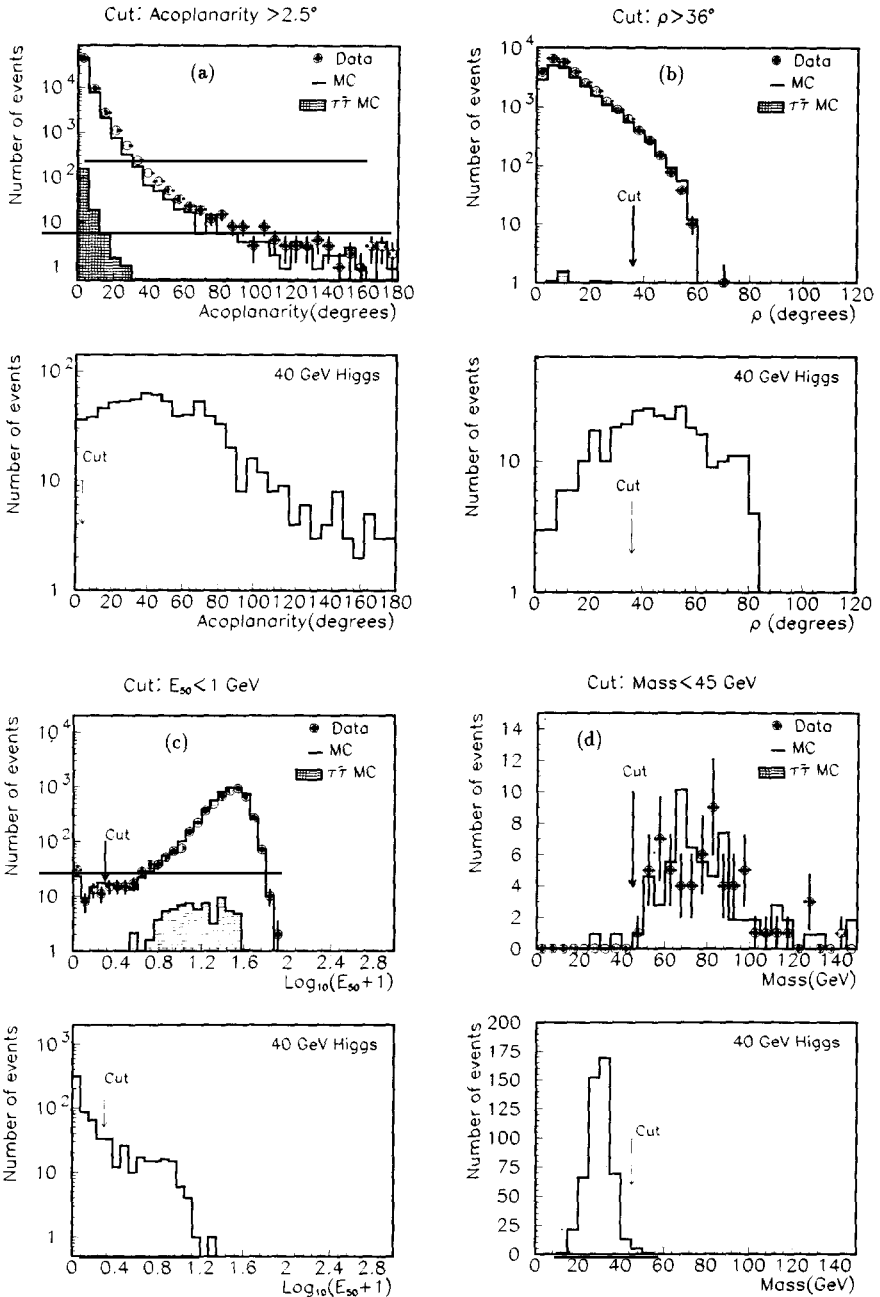Fig. 1. The sequential selections for $H^0\nu\bar{\nu}$ analysis I for data (dots) compared with simulated (histogram) initially normalised $Z^0 \to q\bar{q}$, $\tau^+\tau^-$ and $Z^0 \to H^0\nu\bar{\nu}$ with $m_{H^0} = 40$ GeV/c^2: (a) ρ, the complement of the smallest angle between jets (only for events with three or more jets); (b) λ, the angle between the missing momentum and the nearest jet; (c) acoplanarity; (d) measured mass of possible H^0 decay products.

Fig. 2. The sequential selections for $H^0 \nu \bar{\nu}$ analysis II for data (dots) compared with simulated (histogram) initially normalised $Z^0 \to q\bar{q}$, $\tau^+ \tau^-$ and $Z^0 \to H^0 \nu \bar{\nu}$ with $m_{H^0} = 40$ GeV/c^2; (a) acoplanarity; (b) ρ, the smallest angle between jets, for events with 3 or more jets; (c) E_{50}, energy in 50° cone opposite missing momentum, only data with E_{50} below 1 GeV is kept; (d) measured mass of possible H^0 decay products.

Standard Model H^0 production: for various masses in GeV/c^2, selection efficiencies ϵ, and expected number of events n

m_{H^0}	$H^0 \nu \bar{\nu}$		$H^0 e^+ e^-$		$H^0 \mu^+ \mu^-$		τ channel	
	$\epsilon\%$	n	$\epsilon\%$	n	$\epsilon\%$	n	$\epsilon\%$	n
12	24	12.91	38	3.22	68	6.12	15	1.51
15	28	11.60	45	2.85	69	4.62	16	1.18
20	38	9.71	45	1.81	68	2.88	19	0.90
25	51	8.39	45	1.15	68	1.83	24	0.64
30	56	5.94	45	0.74	66	1.13	27	0.49
35	59	3.91	47	0.48	65	0.70	26	0.30
40	58	2.35	45	0.28	67	0.44	29	0.21
45	45	1.05	42	0.15	65	0.25	28	0.12
50	30	0.40	44	0.09	63	0.14	27	0.06

No events from the real data passed these selections in *analysis I*. There was one remaining background candidate among the Monte Carlo $Z^0 \to q\bar{q}$ decays, with an energetic, isolated photon pointing towards a region (around 40°) where photon detection is absent.

In analysis II the comparison of the differential distributions for the simulated backgrounds and possible H^0 signal led to the following selections:
(a) acoplanarity above 2.5°, fig. 2a;
(b) ρ above 36° for events with more than two jets, fig. 2b;
(c) E_{50} below 1 GeV, fig 2c;
(d) m_τ below 45 GeV/c^2, fig. 2d.

Again no events from the real data passed these selections, while two events from the simulated background $Z^0 \to q\bar{q}$ were selected. One was the same as in analysis I, the other had both a large initial-state radiation and a jet pointing towards the region (around 40°) where neutral particle detection is poor. When normalised by the sample sizes, the two Monte Carlo events correspond to an expected background of 1.8 ± 1.3 events.

Accepting all events in both analyses results in the detection efficiency for a Higgs boson mass in the range 10 to 50 GeV/c^2 shown in table 2 (and fig. 10a). Systematic errors (typically ± 0.028) were evaluated by comparing the small systematic differences between the data and Monte Carlo differential distributions. The expected number of selected H^0 decays is also shown in table 2 (and fig. 10b).

4. Search for $Z^0 \to H^0 + e^+ + e^-$

The signature for $Z^0 \to H^0 Z^{0*}$, $Z^{0*} \to e^+ e^-$ is two isolated high-energy electrons and some hadrons. Isolation is essential to reject background from semileptonic decays of heavy quarks.

In order to accept as many electrons as possible, this analysis used two different definitions of electrons (with momentum measured by the tracking chambers, p_e, shower energy in the electromagnetic calorimeters, E_e, and residual energy measured by the hadron calorimeter, E_h.) The "firm" electron is distinguished from other charged particles by requiring (a) E_e over 3 GeV, (b) $E_e/|p_e|$ above 0.3 and (c) E_h below 1 GeV. The "loose" electron can be either (a) an electromagnetic shower with E_e above 3 GeV and E_h below 1 GeV, associated with a charged particle or behind an insensitive region between TPC modules, or (b) a charged particle with p_e above 4 GeV/c extrapolating to an insensitive region between HPC modules with E_h above 1 GeV. After selections the main background is from true electrons from other sources rather than from misidentified hadronic showers, so stricter electron identification criteria are not needed.

The electron energies (associated with the extrapolation of the electron track) are augmented by adding the energies of satellite showers, due to bremsstrahlung in the material in front of the calorimeters, within a cone whose opening angle is a decreasing function of the parent shower energy.

We analyse all data when the TPC and the electromagnetic calorimeters were working properly.

An event that could be from $H^0 Z^0 *$ production must come from the interaction region, within 10 cm in the beam direction and within 4 cm in the transverse direction. The event must have two (or more) possible electrons (from the $Z^0 *$), including at least one firm and a second firm or loose electron with opposite charge and 4 or more charged particles with momentum above 500 MeV/c from the H^0 decay. Fig. 3 (and table 3) show the effects of further sequential selections for data and simulated $q\bar{q}$ event initially normalised to the data, as well as for $Z^0 \to H^0 e^+ e^-$ events with $m_{H^0} = 40$ GeV/c^2. Events must have:

(a) one electron energy above 12 GeV and the other shower energy or tracking momentum above 5 GeV, fig. 3a;

(b) the opening angle between the two electrons over 20°, fig. 3b;

(c) the isolation angle between each electron and the closest jet axis over 25°, fig. 3c.

The selection efficiencies shown in table 2 (and fig. 10a) have been calculated by generating samples of Monte Carlo events for different values of the mass of the Higgs boson. A systematic error of 2% on all the efficiencies has been evaluated by varying the selection criteria. Table 2 (fig. 10b) also shows the expected number of events.

The simultaneous requirements of relatively high multiplicity and electron isolation remove background from leptonic Z^0 decays. No background from hadronic events was found in a sample of 120 000 simulated $q\bar{q}$ events.

However one event in the data does have two isolated, high-energy electrons (see table 4). The electrons with momenta 31.5 ± 3.1 and 21.3 ± 2.7 GeV/c are at large angles to the beam and 100° and 43° away from the nearest jets (and 72° and
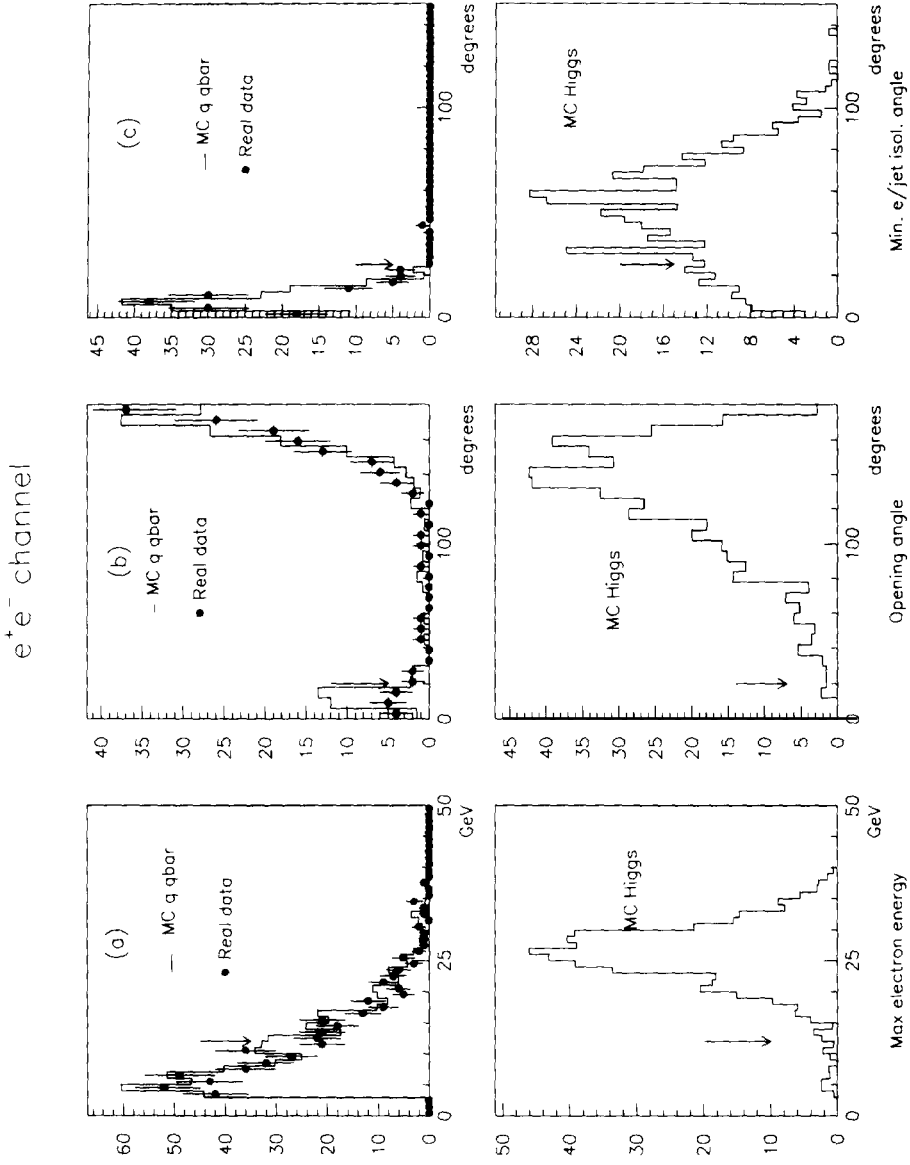
Fig. 3. Distributions showing the effects of the sequential selections on the variables used for the $Z^0 \rightarrow H^0 e^+ e^-$ analysis for data (dots) and simulated (histogram) initially normalised $Z^0 \rightarrow q\bar{q}$ and $H^0 e^+ e^-$ with $m_{H^0} = 40$ GeV/c^2: (a) maximum electron energy; (b) opening angle between the electrons; (c) isolation angle, the minimum angle between an electron and jet.

TABLE 3

The numbers of events remaining after the $Z^0 \rightarrow H^0 e^+ e^-$ sequential selections on the data, and on Monte Carlo background samples normalised to the number of hadronic Z^0 decays in the initial data sample

Selection	Real data	Simulated $Z^0 \rightarrow q\bar{q}$	Simulated 4 fermions	$m_{H^0} = $ 40 GeV/c^2
e identification	508	566	0.63	0.40
e energies	154	169	0.53	0.38
$e^+ e^-$ angle $> 20°$	141	142	0.52	0.38
e-jet angle $> 25°$	1	0	0.39	0.28

$31°$ away from any charged particle with momentum over 300 MeV/c and neutral hadrons above 2 GeV) while the missing mass to the electron pair is 35.4 ± 5.0 GeV/c^2. The measured mass of the two close jets (jets 1 and 2 with 7 charged particles taken as pions) is 9 GeV/c^2. There is evidence of other particles in the direction of the missing momentum, towards the less efficient forward region.

Two particular mechanisms which may simulate the $H^0 e^+ e^-$ final state were studied with larger statistics: $b\bar{b}$ production and the four-fermion processes $e^+ e^- \rightarrow e^+ e^- q\bar{q}$. In order to have statistical precision equivalent to fractions of an event, 800 000 $Z^0 \rightarrow b\bar{b}$ were generated with the Lund Monte Carlo program [18], JETSET. 900 of these events passed wide selections and were submitted to full simulation and reconstructed. Only 2 passed all final selections, corresponding to an expectation of 0.05 ± 0.04 events in our experimental sample.

The four-fermion background has been studied with a simple simulation [20,21] assuming zero-mass fermions. Two-photon processes making $q\bar{q}$ are included. Final-state particles were generated using quark fragmentation from JETSET and submitted to the full detector simulation. The cross section has been calculated as a function of the centre-of-mass energy, after selections that are required by the experimental acceptance or H^0 candidate criteria. These selections avoid infrared divergences in the calculation. The full simulation shows the background to

TABLE 4

$Z^0 \rightarrow H^0 e^+ e^-$ candidate, run 10 600 event 4505, momenta and energies. Missing mass to $e^+ e^- = 35.4 \pm 5.0$ GeV/c^2, m(jets 1, 2) = 9.0 GeV/c^2, m(jets 1, 2, 3) = 17 GeV/c^2

p_x (GeV/c)	p_y (GeV/c)	p_z (GeV/c)	E (GeV)	
4.62	−20.78	−1.98	21.39	e^+
−0.13	22.72	21.84	31.51	e^-
0.04	−6.60	4.89	9.19	jet-1
−4.51	−3.02	1.24	5.89	jet-2
0.58	0.85	−2.81	3.00	jet-3

$Z^0 \to H^0 e^+ e^-$ is $0.39 \pm 0.04 \pm 0.08$ (*syst.*) events (see table 3, column 4) including a reduction factor 0.74 (averaged over the beam energies) to account for the effects of initial-state radiation. The systematic error is due to the theoretical approximations made in the calculation.

Summarizing, the search for $Z^0 \to H^0 e^+ e^-$ gives one candidate and an expected background of 0.44 ± 0.10 events.

5. Search for $Z^0 \to H^0 \mu^+ \mu^-$

The selection of the $H^0 \mu^+ \mu^-$ channel relies on the identification of high-energy, isolated muons, which distinguish H^0 production from semi-leptonic decays of $b\bar{b}$ pairs.

Pairs of muons are selected using different criteria for the two particles. The first "firm" muon is selected by a good match in space between the extrapolation of a track of a charged particle and a set of hits in at least two detection planes of the muon chambers. In the transverse plane, the distance from the first hit to the extrapolation and the deflection between the set of hits and the extrapolation, are required to be less than five times their intrinsic resolutions due to multiple scattering at small angles. In addition, the energy depositions measured by the electromagnetic and hadron calorimeters must be consistent with those expected for a minimum ionizing particle. This condition is fulfilled by restricting the total shower energies as well as the energy depositions in each part of the calorimeters.

In order to select as many muon pairs as possible, the second "loose" muon is allowed to fail the conditions for muon chambers hits, or for the energy deposits in the calorimeters. The single muon selection efficiencies were monitored on real and simulated $\mu^+ \mu^-$ events as well as on real $\tau^+ \tau^-$ events where one τ decays into one charged particle while the other decays into three particles. These τ decays were also used to estimate the expected pion contamination. The results are given in table 5 with the corresponding statistical uncertainties. Requiring one

TABLE 5

Efficiency for μ identification (in %)

Efficiencies and contamination	Firm identification	Loose identification
efficiency from real $\tau^+ \tau^-$ events	88.4 ± 9.0	95.3 ± 9.5
efficiency from real $\mu^+ \mu^-$ events	89.1 ± 0.4	96.7 ± 0.2
efficiency from simulated $\mu^+ \mu^-$ events	92.4 ± 0.4	98.2 ± 0.2
π taken as μ from real $\tau^+ \tau^-$ events	2.1 ± 0.5	4.4 ± 0.7

"firm" and one "loose" muon identification leads to a high dimuon selection efficiency and a small pion contamination. The simulation is found to be in agreement with the data to within 3%.

Candidates for $Z^0 \to H^0 \mu^+ \mu^-$ are selected by requiring events with six or more charged particles (including the two muons) coming from the interaction region, within 10 cm along the beam direction and within 5 cm in the transverse plane. This selection eliminates radiative events with the photon producing a shower at the beam pipe or when entering the detector. In such events, the tracks coming from the shower do not extrapolate back to the beam crossing with the same accuracy as particles produced at the Z^0 decay. This type of background can therefore be reduced by requiring that all tracks taken into account in the charged multiplicity come from the interaction region.

Furthermore, the two muons must have opposite charges and momenta above 5 GeV/c, while their opening angle has to be larger than 30° in order to suppress the contribution from sequential leptonic decays of b-quarks. A set of kinematical cuts is then applied to further reduce the contamination from $b\bar{b}$ decays. These selections take advantage of the fact that muons produced in association with a Higgs boson are expected to be isolated and of high momentum, unlike those coming from the decay of a b-quark. Fig. 4 and table 6 show the effects of these sequential selections on data and simulated $q\bar{q}$ events initially normalized to the data, as well as on $Z^0 \to H^0 \mu^+ \mu^-$ events with $m_{H^0} = 40$ GeV/c^2. The following conditions are required:

(a) momentum of one muon, μ_1, above 15 GeV/c, fig. 4a;
(b) transverse momentum of μ_1 over 5 GeV/c with respect to the thrust axis of the system recoiling from the dimuon, fig. 4b;
(c) transverse momentum of the other muon, μ_2, over 3 GeV/c with respect to the same axis as in (b), fig. 4c;
(d) angle between μ_1 and the closest jet above 30°, fig. 4d;
(e) angle between μ_2 and the closest jet above 10°, fig. 4e.

The Higgs selection efficiency, shown in table 2 and fig. 10a, is almost independent of m_{H^0}. The systematic uncertainties are dominated by a 4% relative uncertainty in the dimuon selection efficiency. The expected number of events is shown in table 2 and fig. 10b.

A background study was made on samples of some 110 000 $Z^0 \to q\bar{q}$, 11 000 $Z^0 \to \tau^+ \tau^-$ (see table 6, columns 3 and 4) and 22 000 $Z^0 \to \mu^+ \mu^-$ decays. A sample of 3000 $Z^0 \to b\bar{b}$ decays with at least one muon in the final state was also used to study the expected background from hadronic Z^0 decays with a higher statistical precision. No events in these samples passed the selections. The four-fermion background was studied using the procedure already described in sect. 4. Final states with one pair of muons and either one pair of quarks, taus or electrons were taken into account. For each final state, a sample of a few hundreds of events was generated and passed through the reconstruction and analysis chain. The

background from $\mu^+\mu^- e^+ e^-$ is small: 0.003 ± 0.002 events. The contribution from $\mu^+\mu^- q\bar{q}$ final states is 0.43 ± 0.02 events, while the background from $\mu^+\mu^-\tau^+\tau^-$ is 0.052 ± 0.007 events. Table 6, column 5, summarises the effect of the selections
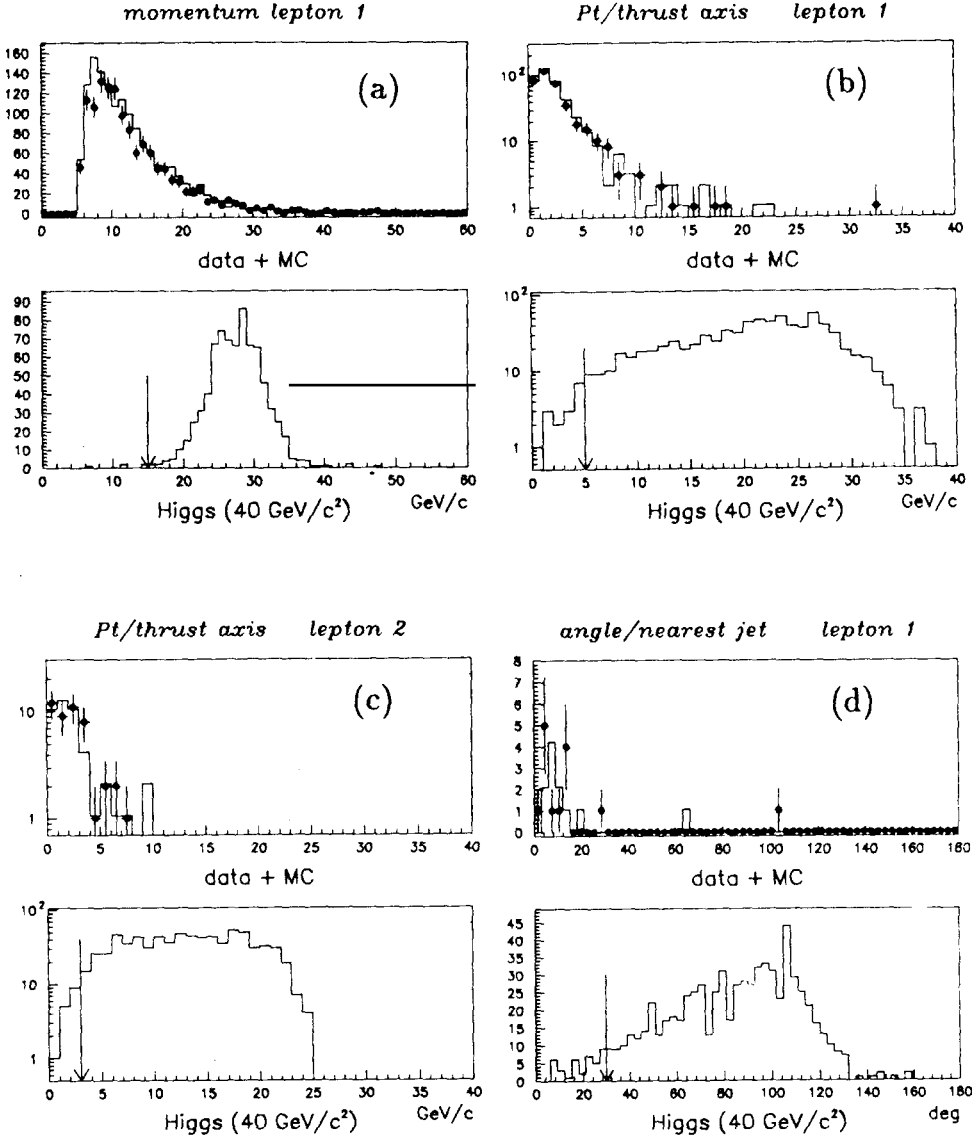

Fig. 4. Distributions showing the effects of the sequential selections on the variables used for the $Z^0 \to H^0\mu^+\mu^-$ analysis for samples of data (dots), simulated (histogram) $Z^0 \to q\bar{q}$ (initially normalised to the data) and simulated $H^0\mu^+\mu^-$ with $m_{H^0} = 40$ GeV/c^2: (a) highest muon momentum; (b, c) transverse momenta of the faster and slower muons with respect to the thrust axis of the system recoiling from the dimuon; (d) the angle between the faster muon and the nearest jet.

TABLE 6

The numbers of events remaining after the $Z^0 \to H^0 \mu^+ \mu^-$ sequential selections on data, simulated $H^0 \mu^+ \mu^-$ events with $m_{H^0} = 40$ GeV/c^2 and simulated backgrounds. The Monte Carlo data are normalised to the number of hadronic Z^0 decays in the initial data sample

Selection	Real data	Simulated $Z^0 \to q\bar{q}$	Simulated $Z^0 \to \tau\tau$	Simulated 4 fermions	$m_{H^0} =$ 40 GeV/c^2
preselections	1331	1506	10.20	0.74	0.50
$p^{\mu_1} > 15$ GeV/c	375	409	7.65	0.57	0.50
$p_t^{\mu_1} > 5$ GeV/c	46	46	0	0.54	0.49
$p_t^{\mu_2} > 3$ GeV/c	14	12	0	0.51	0.48
$\theta(\mu_1 \text{ jet}) > 30°$	1	1	0	0.50	0.46
$\theta(\mu_2 \text{ jet}) > 10°$	0	0	0	0.48	0.44

on four-fermion events. The total expected background in the $H^0 \mu^+ \mu^-$ channel is $0.48 \pm 0.02 \pm 0.10$ (*syst.*) events.

Finally, to further check our background computation, we relaxed the selection on the impact parameter of tracks taken into account in the charged multiplicity, allowing impact parameters up to 20 cm along the beam direction and up to 10 cm in the transverse plane. One event was then selected in the data. In this event, most of the charged particles recoiling from the dimuon form a narrow jet, with low mass, pointing in the forward direction to an electromagnetic shower of 9 GeV. This jet can either be due to a photon conversion at the beam pipe or a primary low mass e^+e^- pair. With these relaxed selections, the additional contri-
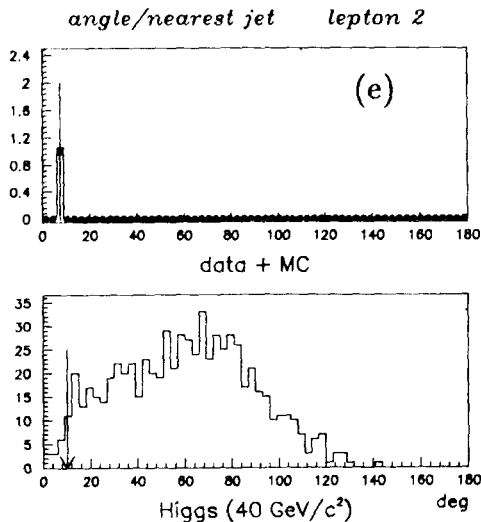

Fig. 4. (e) The angle between the slower muon and the nearest jet.

bution from radiative $Z^0 \to \mu^+\mu^-$ decays is 0.33 ± 0.23 events, while the other backgrounds remain practically the same.

6. Search for H^0 production with final-state $\tau^+\tau^-$ pair

According to the Standard Model final states with isolated tau decays can be produced both by Z^0 decay and by H^0 decay (see table 7). A τ decay candidate is a "slim" jet with low multiplicity and intermediate energy. Our analysis does not look for identified electrons or muons but any charged particles, so we use all runs in which the main tracking device, TPC, is working.

Selected events must have at least two slim jets (with one to three charged particles with $|p|$ above 300 MeV/c made into jets using LUCLUS) and two or more other charged particles. Variables χ and ψ are introduced to reduce the background from $Z^0 \to q\bar{q}$. Both use the measured energies, E^{ch}, of charged particles. The quantity $\chi = |(E^{ch}_{jet_2} - E^{ch}_{jet_1})/E^{ch}_{jet_2} + E^{ch}_{jet_1})|$ measures the relative energies of exactly two jets constructed from all the charged particles that are not included in the two τ candidates. The quantity $\psi = (E^{ch}_{\tau_1} + E^{ch}_{\tau_2})/E_{heml}$ is the ratio between the energy of the two τ candidates and the total energy of the charged particles in the hemisphere (with axis along $p_{\tau_1}/|p_{\tau_1}| + p_{\tau_2}/|p_{\tau_2}|$) that contains them.

A study of the differential distributions for the simulated $Z^0 \to q\bar{q}$ and $Z^0 \to \tau^+\tau^-$ background lead to selections that optimise background rejection and H^0 acceptance. Details (see below) are given in table 8 for data and simulated $q\bar{q}$ events and $Z^0 \to Z^0*(\to \tau^+\tau^-)H^0$ with $m_{H^0} = 40$ GeV/c^2.

The first τ candidate is required to have only one charged particle.

After this selection only 7 real events and 6 simulated $Z^0 \to q\bar{q}$ events (no simulated $Z^0 \to \tau^+\tau^-$) have a second slim jet with one charged particle (the 1–1 topology.) After further selections to reduce background (χ below 0.6, ψ above 0.6, and sphericity above 0.2) no events remain.

If the second slim jet has two or three charged particles (the 1–2 and 1–3 topologies) then other sequential selections are used, see table 8 and fig. 5. Events must have:

TABLE 7

Standard Model H^0 production with final-state $\tau^+\tau^-$ pair: branching ratios and detection efficiencies for $m_{H^0} = 40$ GeV/c^2

Decays	Branching ratio	Efficiency
$Z^0 \to Z^0*(\to \tau^+\tau^-)H^0$	3.3%	11%
$Z^0 \to Z^0*(\to q\bar{q})H^0(\to \tau^+\tau^-)$	70.9% × 6%	11%
$Z^0 \to Z^0*(\to \ell^+\ell^-)H^0(\to \tau^+\tau^-)$	3.3% × 6%	26%

TABLE 8

The numbers of events remaining after the $Z^0 \to H^0 \tau^+ \tau^-$ sequential selections on the data and on Monte Carlo background samples normalised to the number of hadronic Z^0 decays in the initial data sample

Selection	Real data	Simulated $Z^0 \to q\bar{q}$	MC 4f	$m_{H^0} = $ 40 GeV/c^2
1–1 topology	7	6	0.35	0.22
$\chi \leqslant 0.6$	5	4	0.30	0.17
$\psi \geqslant 0.6$	3	3	0.29	0.16
sphericity $\geqslant 0.2$	0	0	0.08	0.13
1–2 and 1–3 topologies	143	120	0.21	0.34
6 GeV $\leqslant E_r \leqslant$ 22.5 GeV	42	41	0.09	0.17
τ opening angle $\geqslant 90°$	25	22	0.06	0.15
$\psi \geqslant 0.8$	19	15	0.05	0.10
sphericity $\geqslant 0.25$	0	0	0.02	0.08

(a) energies of both slim jets above 6 GeV and below 22.5 GeV, fig. 5a;
(b) opening angle between them above 90°, fig. 5b;
(c) ψ above 0.8, fig. 5c;
(d) sphericity above 0.25, fig. 5d.

The simulated $Z^0 \to q\bar{q}$ sample is normalized to the real events in table 8 and figure 5 after preliminary selections.

After the selections no candidates remain in the data or simulated $Z^0 \to q\bar{q}$ or $Z^0 \to \tau^+\tau^-$ decays, while we expect $0.21 \pm 0.02 \pm 0.02$ events when m_{H^0} is 40 GeV/c^2 (see table 2). Systematic errors were evaluated by changing the selections.

Contributions from backgrounds from four fermion processes giving all $\ell^+\ell^-$ $q\bar{q}$ and $\tau^+\tau^-\ell^+\ell^-$ final states have been evaluated. After the selections we expect $0.10 \pm 0.2 \pm 0.02$ background events (see table 8 column 4).

Results of the search for the Standard Model Higgs particle are summarized in sect. 9.

7. Search for MSSM neutral Higgs decaying to $\tau^+\tau^-$

The search for MSSM h^0 or A^0 (see sect. 1) decaying to $\tau^+\tau^-$ looks for two isolated τ decays accompanied by two heavy quark jets. This search for MSSM decays is different from the above search for the Standard Model $H^0 \to \tau^+\tau^-$. It includes both charged and neutral particles and uses different selections. Results of both analyses have been cross-checked and agree. Slim jets are defined as having up to three charged particles and are selected as candidates for τ decays. No restriction is made on their neutral multiplicity but their mass must be below 2.5 GeV/c^2.

The search is restricted to four-jet events (using LUCLUS) with thrust below 0.9. The number of charged particles included in the slim jets is shown in fig. 6 for
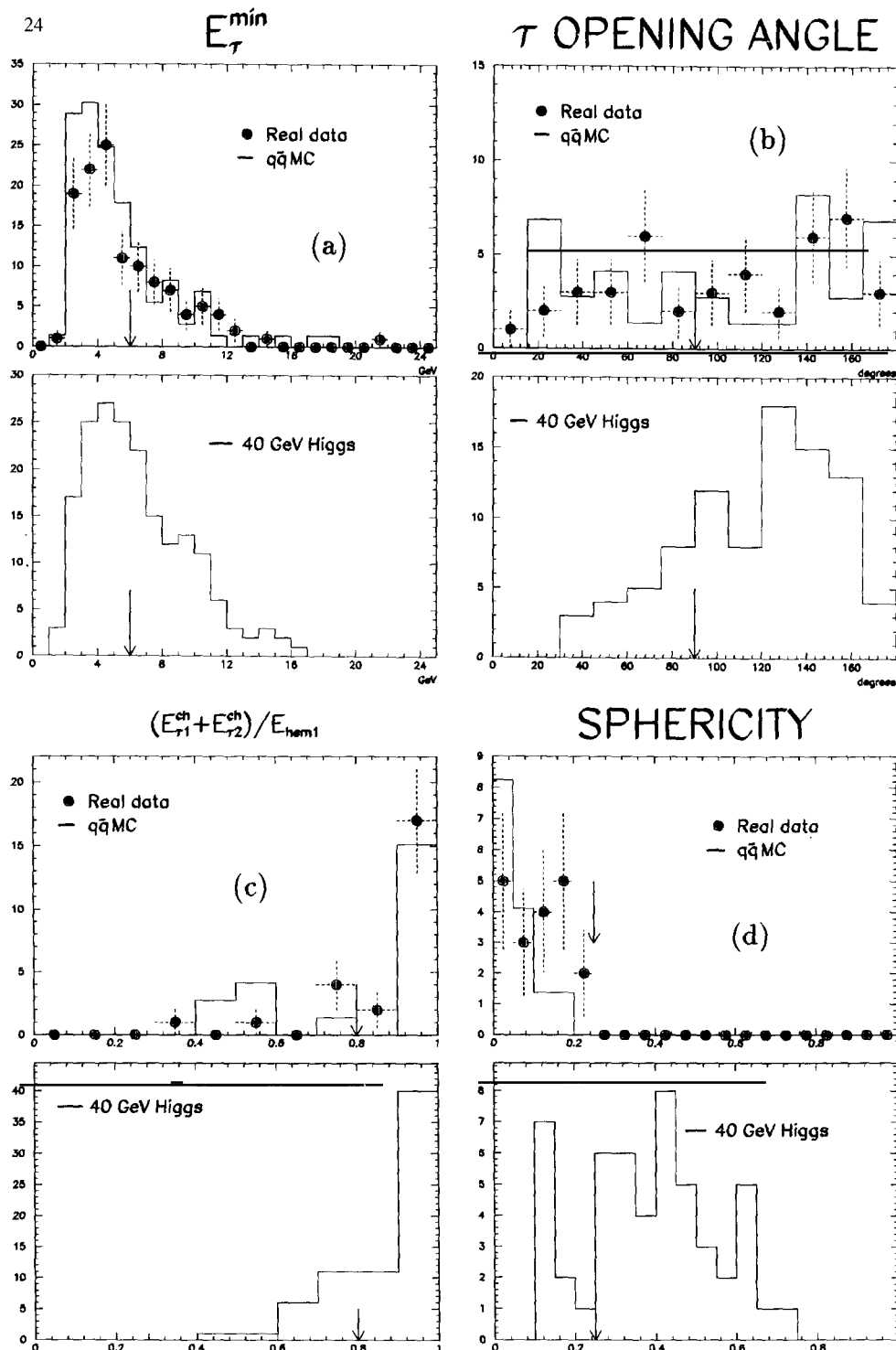
Fig. 5. Distributions showing the effects of the sequential selections on the variables used for the $Z^0 \to H^0 \tau^+ \tau^-$ analysis when the second slim jet has 2 or 3 charged particles: data (dots) and simulated (histogram) initially normalised $Z^0 \to q\bar{q}$ and $H^0 \tau^+ \tau^-$ with $m_{H^0} = 40$ GeV/c^2. (a) Minimum τ energy reconstructed from charged particles; (b) opening angle between the τ; (c) ψ (see text); (d) sphericity.
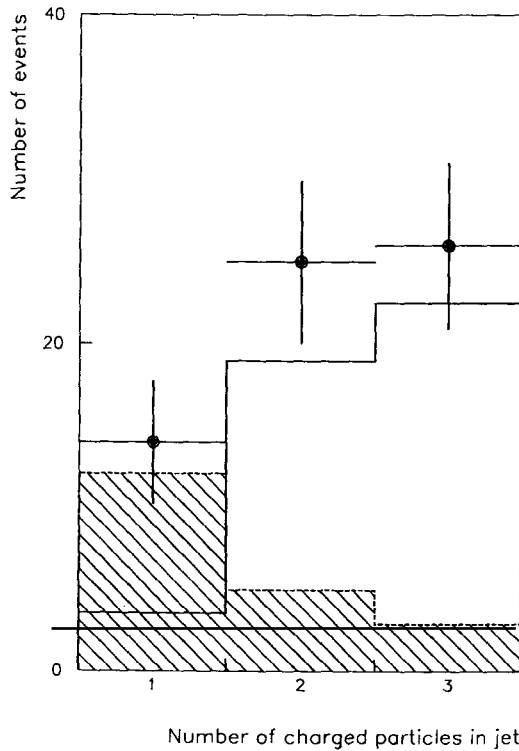
Fig. 6. Charged multiplicity observed in the low-multiplicity jets in four-jet events, for the data (points), simulated (line histogram) initially normalised $Z^0 \to q\bar{q}$ and $Z^0 \to h^0A^0$ for $m_{h^0} = m_{A^0} = 40$ GeV/c^2 (hatched histogram).

the data, simulated $Z^0 \to q\bar{q}$ decays initially normalised to the data and $Z^0 \to h^0A^0$. As expected, slim jets with three charged particles dominate the background while jets with a single charged particle dominate the possible signal. We therefore apply different selections according to the topology of the τ decays.

Two of the jets must be slim jets. The first slim jet is required to have only one charged particle, E^{ch} above 2 GeV, and total energy above 3 GeV (including any neutral particles). When (a) the second slim jet also has one charged particle, one of the slim jets must have E^{ch} above 3 GeV. When (b) the second jet has two charged particles, it must have E^{ch} above 1 GeV. When (c) the second jet has three charged particles, both jets must have E^{ch} above 3 GeV.

The two slim jets (τ candidates) have a large opening, θ_l. The cosine of this is plotted in fig. 7a against $\cos \theta_h$ (the angle between the high-multiplicity jets) for the selected real events (black circles), and in fig. 7b for simulated $Z^0 \to h^0A^0$ decays with $m_{h^0} = m_{A^0} = 40$ GeV/c^2. A concentration is seen for the simulated h^0A^0 (black squares) about $\cos \theta_l$, $\cos \theta_h \approx -0.6$ but no similar structure is seen for the data. No events in the data have both $\cos \theta$ between -0.8 and -0.2, where about 1 background event (open circles) is expected.
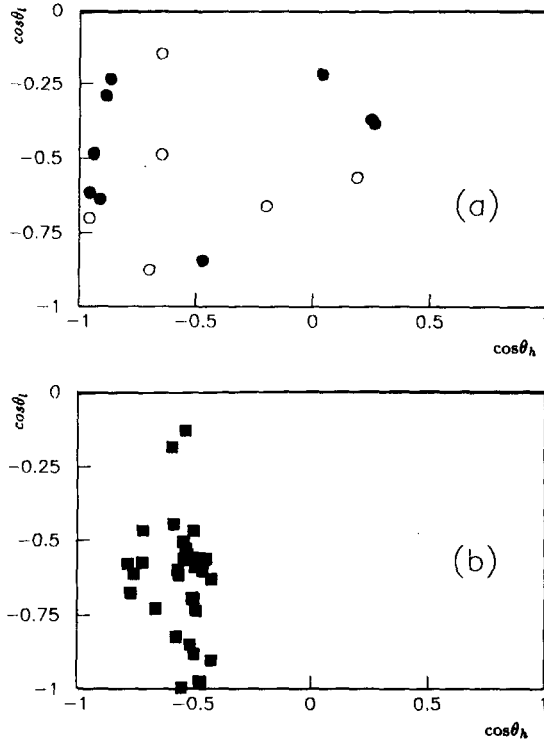
Fig. 7. Distribution of $\cos \theta_\ell$ versus $\cos \theta_h$ where θ_ℓ (θ_h) is the angle between the two low- (high-) multiplicity jets for (a) data (black circles) and simulated $Z^0 \to q\bar{q}$ (open circles); (b) simulated $Z^0 \to h^0 A^0$ decays for $m_{h^0} = m_{A^0} = 40 \text{ GeV}/c^2$.

The efficiency for finding $Z^0 \to h^0 A^0$ decays by these selections is $12 \pm 2\%$ and varies very slowly for m_{A^0} between 35 and 42 GeV/c^2.

If f_1 is the branching ratio for $Z^0 \to h^0 A^0$ and f_2 the branching ratio for $h^0 A^0 \to \tau\tau + 2\text{jets}$, then the absence of events means $f_1 \cdot f_2 < 2.5 \times 10^{-4}$ at the 95% confidence level. Fig. 11, contour B, shows the corresponding MSSM limit in the $(m_h, \tan \beta)$-plane, assuming values for f_1 and f_2 calculated from the formulae defined in sect. 1.

8. Search for MSSM neutral Higgs decaying to 4 jets

The MSSM Higgs h^0 and the A^0 also decay to purely hadronic final states (see sect. 1) and may be reconstructed from their decay products. In order to study the

expected mass resolutions and detection efficiencies, we simulated $Z^0 \rightarrow h^0 A^0$ decays with various combinations of masses (m_h, m_A), for both tan β above and below 1. Decays of the h^0 and the A^0 into $c\bar{c}$, $\tau^+ \tau^-$ and $b\bar{b}$ were given branching ratios predicted by the MSSM. Subsequent hadronization used parton shower evolution and string fragmentation from the Lund Monte Carlo program [18]. The data analysis required the simultaneous operation of the TPC, OD and HPC at a high-quality level.

First, all hadronic events with a visible energy larger than 20 GeV are reconstructed as four-jet events (if possible), using an iterative procedure based on maximization of 4-thrust [22] (a generalization of thrust to the case of four-jet axes). The jets are reconstructed from the measured charged particles (with momentum above 0.1 GeV/c, fractional momentum error below 1, and $|\cos \theta|$ below 0.93, where θ is the polar angle) and reconstructed electromagnetic calorimeter clusters in the HPC (with $|\cos \theta|$ below 0.8). Noisy channels are removed from the electromagnetic calorimeter signals by an algorithm which removed less than 1% of the solid angle. This has a negligible effect on the jet finding efficiency. Each jet was required to consist of at least four particles.

Next, in order to improve the jet–jet mass resolution, a constrained fit is performed, in which the measured jet energies and momenta are corrected, using the constraints from energy and momentum conservation. The twelve fitted parameters are chosen in such a way that their distributions in simulated $Z^0 \rightarrow h^0 A^0$ are nearly gaussian. For each jet they are a_j, the log of a rescaling coefficient, e^{a_j}, applied to the energy and momentum of the jet, and two momentum components, b_j and c_j, transverse to the measured jet direction. The mean value of a_j is $(0.14 + 0.5 \cos^2 \theta_j)$, where θ_j is the polar angle of the jet axis with respect to the beam. Similarly, the gaussian widths of the parameters used in the fit are $\sigma(a_j) = (0.26 + 0.21 \cos^2 \theta_j)$ and $\sigma(b_j) = \sigma(c_j) = 1.9$ GeV/c. The χ^2 of the fit had to be smaller than 20. Only minor differences were found between the simulated decays in regions with tan β above and below 1.

After the fit, each of the three pairs of di-jet masses that can be formed is entered in a plot of the smaller di-jet mass, m_S, versus the larger di-jet mass, m_L.

Since the main background comes from $Z^0 \rightarrow q\bar{q}$ decays, selections are made on the minimum opening angle, θ_{ij}^{min}, and the minimum jet energy, E_k^{min}, among the four reconstructed jets. Fig. 8a shows the distribution of θ_{ij}^{min} plotted against E_k^{min} for simulated $Z^0 \rightarrow q\bar{q}$ subjected to the same analysis (with arbitrary normalisation), and fig. 8b $Z^0 \rightarrow h^0 A^0$. From such comparisons, and the MSSM branching ratio for $Z^0 \rightarrow h^0 A^0$, the statistical significance of a possible signal in the mass region above 25 GeV/c^2 is optimized by requiring $\theta_{ij}^{min} \times E_k^{min}$ larger than 9 rad GeV (the curve on fig. 8).

The resulting plot of m_S against m_L is shown in fig. 9a for the data and in fig. 9b for simulated decays with $m_h = 30$ GeV/c^2 and $m_A = 35$ GeV/c^2, where events generated with tan β above and below 1 have been combined. The simula-
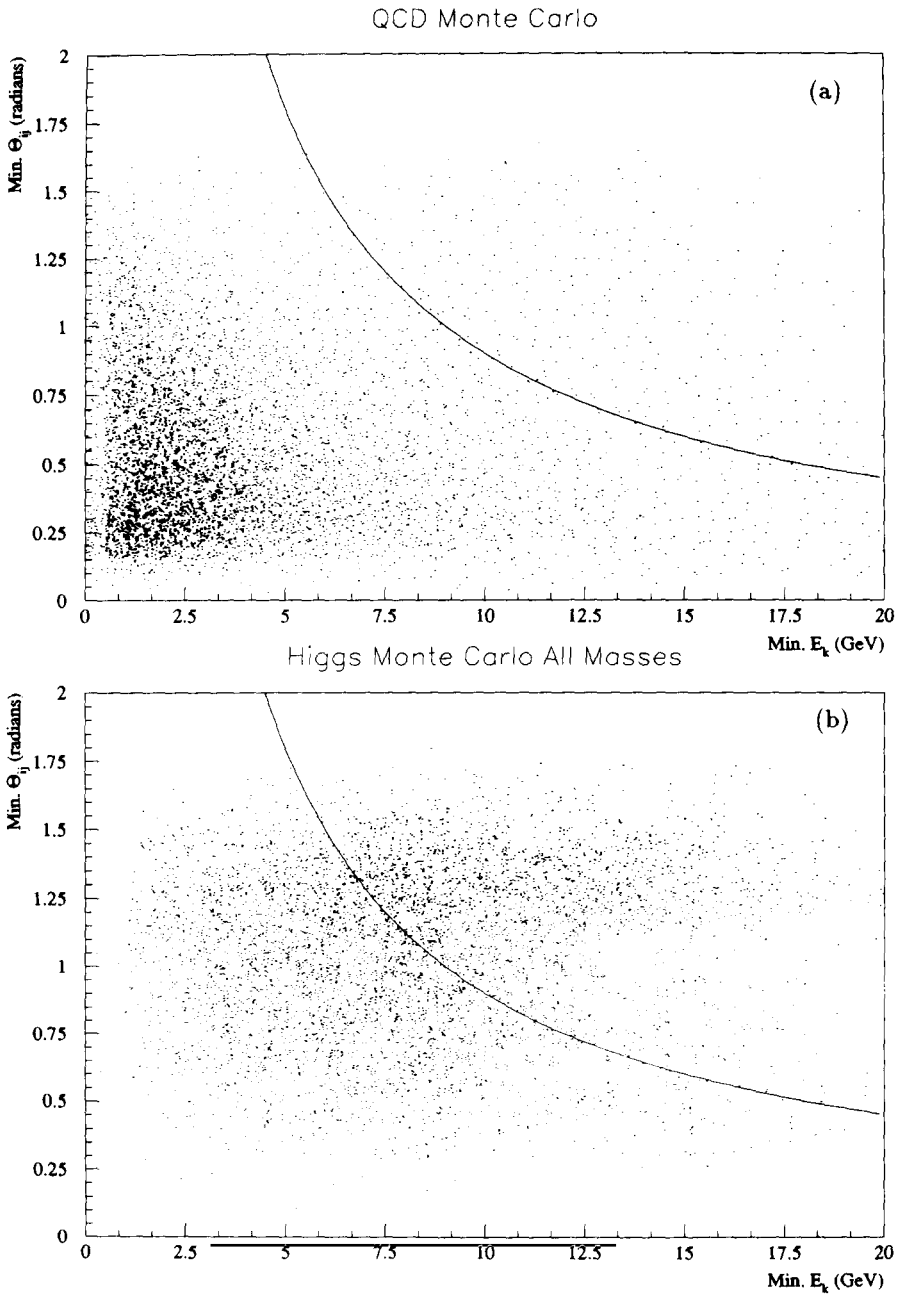
QCD Monte Carlo

Higgs Monte Carlo All Masses

Fig. 8. The minimum angle between jets in the MSSM four-jet analysis θ_{ij}^{min}, plotted against minimum jet energy, E_k^{min}, for (a) simulated $Z^0 \rightarrow q\bar{q}$, and (b) simulated h^0A^0. Data above the curve are selected in the analysis.
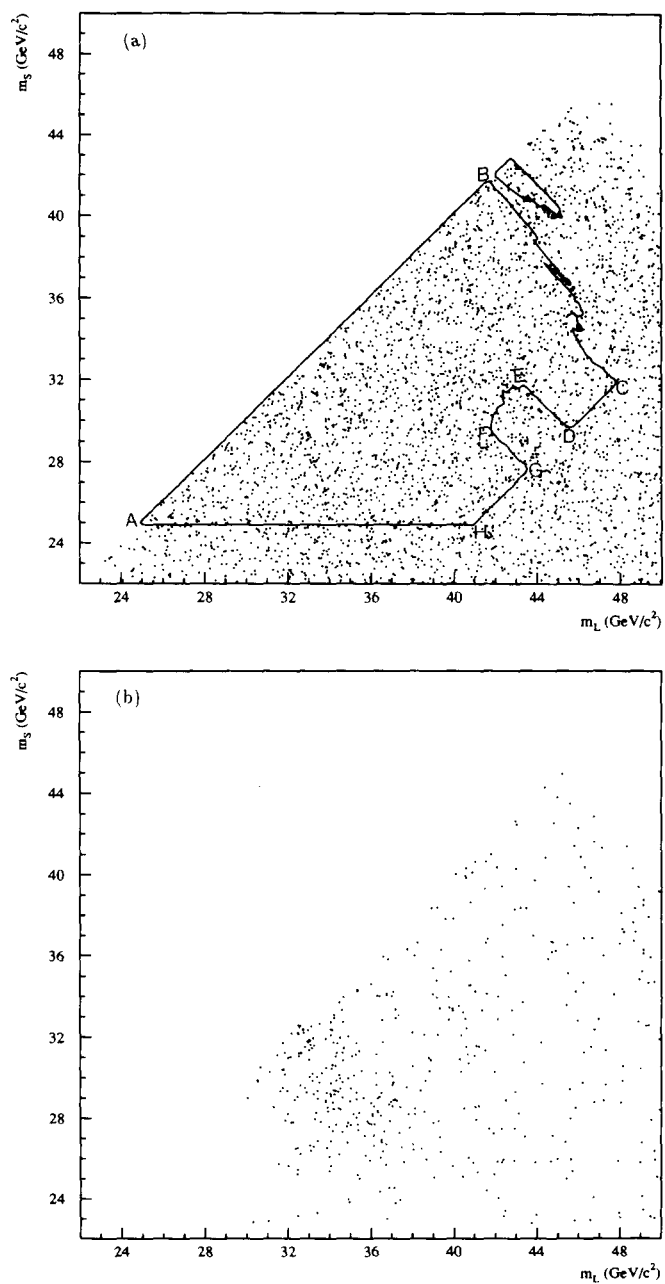
Fig. 9. The smaller di-jet mass in the MSSM four-jet analysis, m_S, plotted against the larger, m_L, for (a) the data, (b) simulated $m_h = 30$ GeV/c^2 and $m_A = 35$ GeV/c^2. In (a) the region within the contour in the (m_h, m_A) plane is excluded at the 95% confidence level.

TABLE 9
Detection efficiency for $Z^0 \to 4$ jets

m_h (GeV/c^2)	m_A (GeV/c^2)	Efficiency (%)
25	40	20.2 ± 1.4
30	35	22.2 ± 1.5
30	45	13.0 ± 1.1
35	40	20.8 ± 1.4
35	50	12.2 ± 1.1
40	45	16.5 ± 1.3

tion shows an accumulation at about the correct masses, surrounded by a wider distribution due to the other jet–jet combinations.

The Higgs boson signal would be a cluster of events in fig. 9a since simulated $Z^0 \to q\bar{q}$ events show a smooth variation with mass. Whereas the jet–jet mass resolution is typically around 2 GeV/c^2 at lower masses, the Monte Carlo studies show that the signal becomes distorted when the kinematical limit is approached. The search for the signal is therefore made in a rectangular window in the $(m_L - m_S, m_L + m_S)$ plane, with constant window area (corresponding to 36 (GeV/c^2)^2 in fig. 9) with sides that depend on the position in the plane. The background is computed by extrapolating from the observed distribution itself, averaged over a region of the same size adjacent to the window. Hence the results do not depend on the simulated $Z^0 \to q\bar{q}$. The efficiencies for finding h^0 and A^0 at masses examined here are shown in table 9.

The expected number of signal events in the search window is calculated from the cross section for h^0A^0 production, and a smooth interpolation of the efficiencies shown in table 9. The efficiencies take into account the part of the signal spilling into the region used to estimate the background. The confidence level corresponding to the calculated signal, given the observed number of events and the estimated background, is then calculated, using Poisson statistics, and the contour corresponding to 95% confidence is located.

The resulting limit on the masses of the h^0 and A^0 is shown in fig. 9 as a contour in the (m_h, m_A) plane (95% confidence level). The straight line AB is because the larger mass is plotted as m_A. The contour between B and C is where $Z^0 \to h^0A^0$ production is limited by the cross section (the small excluded island at $m_h \sim 42$ GeV/c^2, $m_A \sim 43$ GeV/c^2 is not used for the limits quoted). The four-jet search was not made to the right of the line CDGH where the MSSM limit comes from the SM H^0 search (see fig. 11, discussed below). The interesting feature DEFG is where h^0A^0 production cannot be excluded due to fluctuations of the data. Thus $m_h \sim 29$ GeV/c^2, $m_A \sim 43$ GeV/c^2 remains as a possible region for MSSM that may not be excluded by the data analysed here.

Since the mass resolution and efficiency is the same for tan β both above and below 1, the result is valid for both.

The search was optimized for masses above 25 GeV/c^2, but since the exclusion contour that can be derived from the search for the SM Higgs particle (contour A on fig. 11) overlaps with our previously published limits [14] for m_h below 26 GeV/c^2, this leaves no uncovered regions at lower masses.

9. Results and conclusions

Fig. 10b shows the expected number of H^0 events within the Standard Model as a function of m_{H^0}. The total error bar shown includes the uncertainties attributable to systematic changes in the selection criteria for each channel, the Monte Carlo statistics used for H^0 detection efficiencies ($\pm 1.5\%$), and in the computation of expected numbers of H^0 decays for uncertainty in the H^0 production cross section and decay branching ratio ($\pm 2\%$) and normalization to hadronic Z^0 decays($\pm 0.6\%$). Including statistical and systematic uncertainties the total H^0 signal would be $3.27 \pm 0.06 \pm 0.12$ events at 40 GeV/c^2. We lower the expected number of events by one standard deviation (the fitted curve on fig. 10b) before calculating mass limits to allow conservatively for the experimental uncertainties.

The candidate for $Z^0 \rightarrow H^0 e^+ e^-$ is consistent with the total expected background of 1.0 ± 0.2 events in all three $Z^{0*} \rightarrow \ell^+ \ell^-$ channels due to four-fermion processes (or $Z^0 \rightarrow b\bar{b}$ with two leptonic decays). Including the expected background of 1.8 ± 1.3 events in the $Z^{0*} \rightarrow \nu\bar{\nu}$ channel gives the total background of 2.8 ± 1.3 events. Since one event survives the selections, we take it into account to compute the 95% confidence level (see fig. 10b) taking the mass of the candidate H^0 to be between 27.2 and 43.6 GeV/c^2. In this region the maximum signal is 3.9 events at 95% confidence level, using the procedure described in ref. [23], extended to allow for the error on the background. Comparison of the expected signal with the 95% confidence level restricts m_{H^0} to be outside the region 12 to 38 GeV/c^2.

Since masses between 0 and 14 GeV/c^2 has been excluded by our previous results [7,11], there is no Higgs boson with mass between 0 and 38 GeV/c^2 (at the 95% confidence level). This result is in agreement with the conclusions of recent searches [24–26] by the other experiments at LEP.

In MSSM (without higher-order corrections [13]) this limit can be used directly to give contour A on fig. 11. The search for h^0 or A^0 producing τ provides the 95% confidence level contour B on fig. 11. For $m_h \approx m_A$, this restricts m_A to be above 42 GeV/c^2. The contour shows the combined limit, with m_h restricted to be above 34 GeV/c^2, for all tan β above 1. The search for four jets from h^0 and A^0 gives the 95% confidence level contour C on fig. 11, when the mass limits are transformed from fig. 9 into the (m_h, tan β) plane. For tan β above 1, the limit C (from four jets) would be slightly less restrictive than the limit B from τ decays. For tan β between 0.3 and 0.5, m_h can be as low as 29 GeV/c^2.
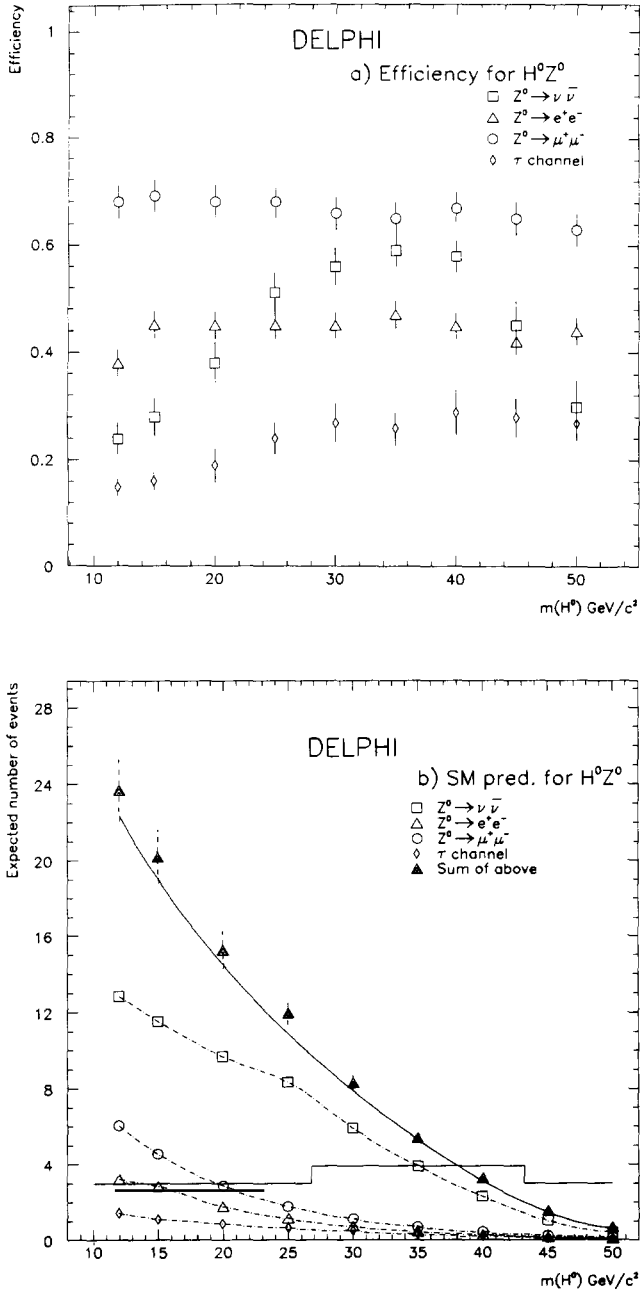
Fig. 10. Standard Model H^0 decays expected for $e^+e^- \to H^0Z^{0*}$ with $Z^{0*} \to \nu\bar{\nu}$ (squares), e^+e^- (triangles), $\mu^+\mu^-$ (circles) and $\tau^+\tau^-$ (diamonds) as a function of m_{H^0}. (a) Efficiencies for detecting H^0. (b) Expected number of detected decays and their sum. The sum is reduced by one standard deviation (the curve) to calculate mass limits. The horizontal line with a step is the 95% confidence level for the analysis with the candidate and backgrounds discussed in the text.
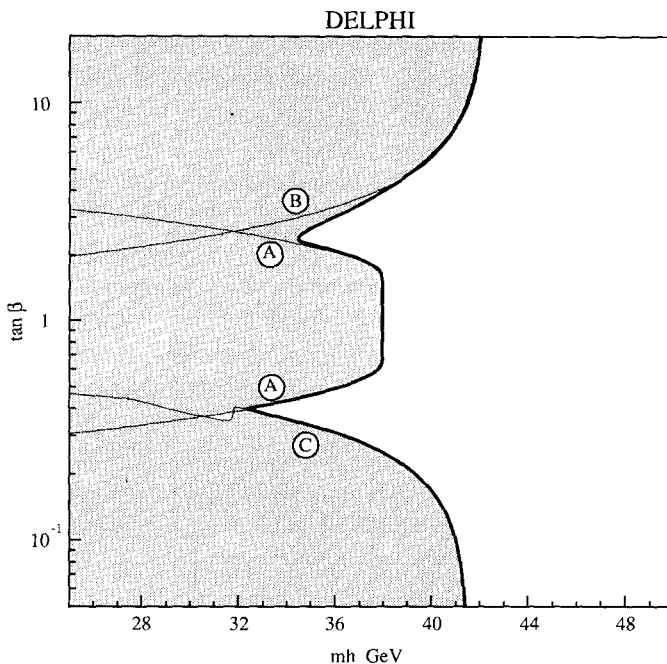
DELPHI

Fig. 11. In MSSM the shaded region in the (tan β, m_h) plane is excluded (at the 95% confidence level, using limits A + B combined and limit C). Contour limits are from searches for: (A) h^0 decays to SM H^0 channels, (B) h^0 or A^0 decays to $\tau^+\tau^-$, (C) h^0 and A^0 giving 4 jets.

As small values of m_h are already excluded in ref. [11], the combination of the contours restricts h^0 and A^0 to masses above 29 GeV/c^2 for tan β between 0.3 and 0.5 (at the 95% confidence level, for MSSM without the higher-order corrections discussed recently [13]) and above 34 GeV/c^2 for all other tan β.

References

[1] S.L. Glashow, Nucl. Phys. (1961) 579;
S. Weinberg, Phys. Rev. Lett. 19 (1967) 1264;
A. Salam, *in* Proc. Nobel Symposium, ed. N. Svartholm (Almqvist and Wiksells, Stockholm, 1968) p. 367
[2] P.W. Higgs, Phys. Lett. 12 (1964) 132; Phys. Rev. Lett. 13 (1964) 508; Phys. Rev. 145 (1966) 1156;
F. Englert and R. Brout, Phys. Rev. Lett. 13 (1964) 321

[3] S.J. Freedman, J. Camp and M. Kroupa, Phys. Rev. Lett. 52 (1984) 240;
    M.J. Savage, B.W. Filippone and L.W. Mitchell, Phys. Rev. Lett. D37 (1988) 1134;
    D. Kohler, B.A. Watson and J.A. Becker, Phys. Rev. Lett. 33 (1974) 1628;
    I. Beltrami et al., Nucl. Phys. A451 (1985) 679;
    R. Barbieri and T.E.O. Ericson, Phys. Lett. B57 (1975) 270
[4] M. Davier and H. Nguyen Ngoc, Phys. Lett. B22 (1989) 533
[5] OPAL Collaboration, M.Z. Akrawy et al., Phys. Lett. B236 (1990) 224; Z. Phys. C49 (1991) 1
[6] ALEPH Collaboration, D. Decamp et al., Phys. Lett. B236 (1990) 233; B241 (1990) 141
[7] DELPHI Collaboration, P. Abreu et al., Nucl. Phys. B342 (1990) 1
[8] ALEPH Collaboration, D. Decamp et al., Phys. Lett. B236 (1990) 233; B245 (1990) 289
[9] OPAL Collaboration, M.Z. Akrawy et al., Phys. Lett. B251 (1990) 211
[10] L3 Collaboration, B. Adeva et al., Phys. Lett. B252 (1990) 518
[11] DELPHI Collaboration, P. Abreu et al., Z. Phys. C51 (1991) 25
[12] H.E. Haber and G.L. Kane, Phys. Rep. 117 (1985) 75;
     J.E. Gunion and H.E. Haber, Nucl. Phys. B272 (1986) 1; B278 (1986) 449;
     H. Pois, T.J. Weiler and T.Ch. Yuan, Nucl. Phys. B347 (1990) 461;
     J.F. Gunion, H.E. Haber, G. Kane and S. Dawson, The Higgs Hunters Guide (Addison-Wesley, Reading, MA, 1990)
[13] Y. Okada, M. Yamaguchi and T. Yanagida, Prog. Theor. Phys. Lett. 85 (1991) 1;
     J. Ellis, G. Ridolfi and F. Zwirner, Phys. Lett. B257 (1991) 83; B262 (1991) 477;
     H.E. Haber and R. Hempfling, preprint SCIPP-90/42;
     R. Barbieri, M. Frigeni and M. Caravaglios, preprint IFUP-TH 46/90
[14] DELPHI Collaboration, P. Abreu et al., Phys. Lett. B245 (1990) 276
[15] DELPHI Collaboration, P. Aarnio et al., Nucl. Instrum. Methods A303 (1991) 233
[16] DELPHI Collaboration, P. Abreu et al., Phys. Lett. B241 (1990) 435; Nucl. Phys. B367 (1991) 511
[17] G. Ekspong and K. Hultqvist, University of Stockholm, USIP report 5 (1982);
     B. van Eijk, DELPHI report 83-84
[18] T. Sjöstrand, Comput. Phys. Commun. 39 (1986) 34;
     T. Sjöstrand and M. Bengtsson, Comput. Phys. Commun. 43 (1987) 367;
     we use JETSET version 7.2 (November 1989)
     The jet finding algorithm LUCLUS is described in
     T. Sjöstrand, Comput. Phys. Commun. 28 (1983) 299
[19] J.D. Bjorken, SLAC report SLAC-198 (1977);
     J. Finford, Phys. Scr. 21 (1980) 143
[20] F.A. Berends and R. Kleiss, Nucl. Phys. B260 (1985) 32
[21] E. Glover, R. Kleiss and J. van der Bij, CERN report CERN-TH5584/89 (1989)
[22] S.L. Wu, Z. Phys. C9 (1981) 329
[23] Particle Data Group, J.J. Hernandez et al., Phys. Lett. B239 (1990) 36
[24] ALEPH Collaboration, D. Decamp et al., Phys. Lett. B246 (1990) 306; Phys. Lett. B265 (1991) 475
[25] OPAL Collaboration, M.Z. Akrawy et al., Phys. Lett. B253 (1991) 511; Phys. Lett. B268 (1991) 122
[26] L3 Collaboration, B. Adeva et al., Phys. Lett. B248 (1990) 203; B257 (1991) 452